



# microRNA-31 regulates skeletogenesis by direct suppression of *Eve* and *Wnt1*



Nina Faye Sampilo<sup>a</sup>, Nadezda A. Stepicheva<sup>b</sup>, Jia L. Song<sup>a,\*</sup>

<sup>a</sup> Department of Biological Sciences, University of Delaware, Newark, DE, 19716, USA

<sup>b</sup> Department of Ophthalmology, University of Pittsburgh School of Medicine, Pittsburgh, PA, 15261, USA

## ARTICLE INFO

### Keywords:

MicroRNA-31  
Sea urchin  
Primary mesenchyme cells  
miRNA target protector  
Post-transcriptional regulation  
Even-skipped  
Vegf signaling  
Wnt

## ABSTRACT

microRNAs (miRNAs) play a critical role in a variety of biological processes, including embryogenesis and the physiological functions of cells. Evolutionarily conserved microRNA-31 (miR-31) has been found to be involved in cancer, bone formation, and lymphatic development. We previously discovered that, in the sea urchin, miR-31 knockdown (KD) embryos have shortened dorsoventral connecting rods, mispatterned skeletogenic primary mesenchyme cells (PMCs) and shifted and expanded *Vegf3* expression domain. *Vegf3* itself does not contain miR-31 binding sites; however, we identified its upstream regulators *Eve* and *Wnt1* to be directly suppressed by miR-31. Removal of miR-31's suppression of *Eve* and *Wnt1* resulted in skeletal and PMC patterning defects, similar to miR-31 KD phenotypes. Additionally, removal of miR-31's suppression of *Eve* and *Wnt1* results in an expansion and anterior shift in expression of *Veg1* ectodermal genes, including *Vegf3* in the blastulae. This indicates that miR-31 indirectly regulates *Vegf3* expression through directly suppressing *Eve* and *Wnt1*. Furthermore, removing miR-31 suppression of *Eve* is sufficient to cause skeletogenic defects, revealing a novel regulatory role of *Eve* in skeletogenesis and PMC patterning. Overall, this study provides a proposed molecular mechanism of miR-31's regulation of skeletogenesis and PMC patterning through its cross-regulation of a Wnt signaling ligand and a transcription factor of the endodermal and ectodermal gene regulatory network.

## 1. Introduction

miRNAs are small non-coding RNAs that play critical regulatory roles as fine-tuners of gene expression to regulate the physiological functions of cells (Bartel, 2009). miRNAs typically bind to the 3' untranslated region (3'UTR) of target mRNAs, silencing translation and/or inducing target mRNA degradation (Bartel, 2009). miR-31, an evolutionarily conserved miRNA, has mostly been examined in the context of various cancers, and limited studies revealed its function in bone homeostasis, myogenesis, auto-immunity (Valastyan and Weinberg, 2010; Yu et al., 2018), lymphatic development (Pedrioli et al., 2010), and embryonic development (Stepicheva and Song, 2015).

Using the purple sea urchin (*Strongylocentrotus purpuratus*), we have previously identified miR-31 to regulate skeletogenesis and patterning of the skeletogenic primary mesenchyme cells (PMCs), by directly suppressing components of the PMC gene regulatory network (GRN) and indirectly regulating the Vegf signaling pathway (Stepicheva and Song, 2015). The molecular mechanism of how miR-31 regulates the Vegf signaling pathway to mediate directed migration of PMCs and skeletal

formation remains unclear. The Vegf/VegfR signaling pathway is critical for the PMCs to form the skeletal rudiment, likely by providing differentiation and chemotactic cues from the ectoderm to the migrating PMCs, as well as activating the transcription of biomineralization genes in the PMCs (Duloquin et al., 2007; Etensohn and McClay, 1986; McIntyre et al., 2014). VegfR10 is expressed specifically in the PMCs and is thought to respond to the Vegf3 ligand expressed in the ectoderm (Adomako-Ankomah and Etensohn, 2013; Duloquin et al., 2007). An overexpression of *Vegf3* leads to supernumerary and abnormal branching of larval skeleton, and loss of *Vegf3* or *VegfR10* results in decreased expression levels of genes involved in biomineralization, such as *p19*, *SM29*, *SM49*, *Msp130*, and a lack of skeleton (Adomako-Ankomah and Etensohn, 2014; Duloquin et al., 2007). Thus, Vegf signaling is critical for various aspects of sea urchin skeletogenesis. Additional signaling pathways, such as non-canonical Wnt (ncWnt), Nodal/BMP, MAPK and PI3 kinase pathways are also important in sea urchin skeletogenesis (Adomako-Ankomah and Etensohn, 2013; Bradham et al., 2004; Croce et al., 2006; Duboc et al., 2004; Schlessinger, 2000).

Conservation of Vegf ligand and receptor recognition between sea urchins and humans has been demonstrated in *Paracentrotus lividus*

\* Corresponding author. 323 Wolf Hall Newark, DE, 19716, USA.

E-mail address: [jsong@udel.edu](mailto:jsong@udel.edu) (J.L. Song).

<https://doi.org/10.1016/j.ydbio.2021.01.008>

Received 15 August 2020; Received in revised form 23 December 2020; Accepted 11 January 2021

Available online 20 January 2021

0012-1606/© 2021 Elsevier Inc. All rights reserved.

### Abbreviations

PMCs	primary mesenchyme cells
GRN	Gene regulatory network
TP	Target protector morpholino
Eve	Even-skipped
Wnt	Wingless-related integration site
Vegf	Vascular endothelial growth factor
DVC	Dorsoventral connecting rods
KD	Knockdown
OE	Overexpression
TF	Transcription factor
cWnt	canonical-Wnt
ncWnt	non-canonical Wnt
EMT	Epithelial to mesenchymal transition
VE	Ventral ectoderm
DE	Dorsal ectoderm
BE-DVM	Border ectoderm-dorsal ventral margin
AP	Anterior-Posterior
DV	Dorsal-Ventral

(*P. lividus*), where *Vegf3* knockdown (KD) resulted in complete loss of skeleton that was rescued by human *VegfA* mRNA (Morgulis et al., 2019). *Vegf* signaling in vertebrates is essential for blood vessel formation and this process has been proposed to be analogous to sea urchin skeletogenesis, since a common set of transcription factors (TFs) (Ets1/2, Erg, Hex, Tel, and FoxO) and signaling pathways (Vegf, Notch, and Angiopoietin) important for vascularization are expressed and utilized in the sea urchin PMCs at the time of skeletal formation (Morgulis et al., 2019).

During the blastula stage, *Vegf3* is likely to be indirectly regulated by *Hox11/13b*, since *Hox11/13b* KD resulted in a complete loss of *Pax2/5/8* and *Wnt5*; and *Wnt5* KD resulted in loss of *Vegf3* expression (McIntyre et al., 2013). *Hox11/13b* activates *Wnt5*, which serves as a short-range signal specifying the border ectoderm (BE) which consists of a ring of ectodermal cells immediately bordering the endoderm anteriorly (McIntyre et al., 2013). In the sea urchin, *Wnt5* binds to an unidentified Frizzled (Fzd) receptor that activates an unidentified activator (McIntyre et al., 2013; Nishita et al., 2010a, 2010b). This unidentified factor, in turn, transcriptionally activates *Pax2/5/8* in the BE (McIntyre et al., 2013). How *Wnt5* signals remains unclear. *Wnt5* is thought to signal primarily through the ncWnt signaling pathway (Nishita et al., 2010a, 2010b). In other contexts, *Wnt5* has also been reported to activate the canonical Wnt/ $\beta$ -catenin (cWnt/ $\beta$ -catenin) pathway (Mikels and Nusse, 2006). The dorsal ventral margin (DVM) is an area in the ectoderm restricted by Nodal signaling in the ventral ectoderm (VE) and BMP signaling in the dorsal ectoderm (DE) (McIntyre et al., 2013, 2014). *Vegf3* is highly expressed at the intersection of *Wnt5* and Nodal/BMP expression at the border ectoderm-dorsal ventral margin (BE-DVM) (McIntyre et al., 2014). *Vegf3*, along with several signaling molecules and TFs, such as *Lim1*, *Nk1*, and *Pax2/5/8*, are restricted to the BE-DVM to provide patterning inputs to the underlying mesenchyme where the PMC ventrolateral clusters reside to form the skeletal rudiments (Adomako-Ankomah and Etensohn, 2013; Duloquin et al., 2007; McIntyre et al., 2013, 2014; Rottinger et al., 2008). Additionally, the expression of *Eve* is important for the activation of *Hox11/13b* (Cui et al., 2014). In the sea urchin, *Eve* is a direct target of the cWnt/ $\beta$ -catenin signaling pathway (Peter and Davidson, 2010, 2011; Ransick et al., 2002). Knockdown of *Eve* in the Veg1 endoderm during the blastula stage resulted in decreased transcript levels of *Hox11/13b*, along with *Wnt1*, *Wnt4*, *Wnt5*, and *Wnt16* (Cui et al., 2014).

Previously, we have shown that most miR-31 KD embryos have mislocalized PMCs that do not express *VegfR10* (Stepicheva and Song, 2015). Interestingly, the *Vegf3* expression domain observed in miR-31 KD

blastulae is expanded and shifted anteriorly (Stepicheva and Song, 2015). We did not bioinformatically identify potential binding sites of miR-31 in *Vegf3* or *VegfR10*, leading us to hypothesize that miR-31 regulates *Vegf3* expression indirectly. The current study reveals that miR-31's direct repression of *Eve* and *Wnt1* indirectly regulates the expression of *Vegf3*. Further, *Vegf3* expression domains correlate with the anterior migration distance of PMCs and the length of skeletal rods. Removal of miR-31's direct suppression of both *Eve* and *Wnt1* recapitulated miR-31 KD induced phenotypes. We also discovered a novel role of *Eve* in regulating skeletogenesis.

## 2. Materials and methods

### 2.1. Animals

Adult *Strongylocentrotus purpuratus* (*Sp*) were obtained from Point Loma Marine Invertebrate Lab, Lakeside, California. Adult males and females were injected with 0.5 M KCl intracoelomically to obtain sperm and eggs. Filtered natural seawater (FSW) (collected from Indian River Inlet; University of Delaware) or artificial seawater (ASW) made from Instant Ocean® was used for embryo cultures incubated at 15 °C.

### 2.2. Cloning

For generating *Eve*, *Wnt1* and *Wnt5* 3'UTR luciferase reporter constructs, PCR primers of *Eve*, *Wnt1* and *Wnt5* 3'UTR sequences were designed based on sequence information available from the sea urchin genome (echinobase.org) (Table S1). Amplified PCR products of *Eve*, *Wnt1* and *Wnt5* 3'UTRs were first cloned into ZeroBlunt vector (Thermo Fisher Scientific, Waltham, MA) and then subcloned into the *Renilla* luciferase (*RLuc*) reporter construct. Mutations were generated within the miR-31 seed sequences using the QuikChange Lightning Kit (Agilent Technologies, Santa Clara, California). The two complete miR-31 seed sites within *Eve* 3'UTR were modified from 5' TCTTGCC 3' to 5' TCCTACC 3' at +28 and +652 positions. The position +1 is the first nucleotide after the stop codon. The truncated miR-31 seed site within *Wnt1* 3'UTR was modified from 5' CTTGCC 3' to 5' CTCGAC 3' at +2482 position. The truncated miR-31 seed site within *Wnt5* 3'UTR was modified from 5' TCTTGC 3' to 5' TCCTAC 3' at +3239 position to disrupt miR-31's binding (Gregory et al., 2008; Stepicheva et al., 2015).

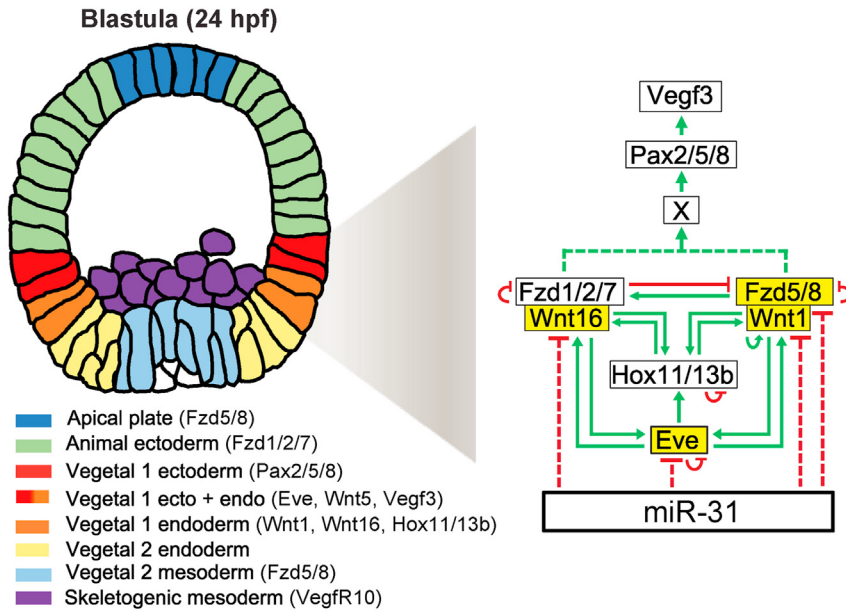
Each of the construct sequences was verified by DNA sequencing (Genewiz, South Plainfield, NJ). Firefly luciferase was used as a normalization control as previously described (Stepicheva et al., 2015). Luciferase constructs containing the *Eve* 3'UTR were linearized with *EcoRI* and luciferase constructs containing *Wnt1* and *Wnt5* 3'UTRs were linearized with *NotI*. The constructs were *in vitro* transcribed using the mMessage machine kit with either T7 (for *Eve*, *Wnt1* and *Wnt5* *RLuc* mRNAs) or Sp6 (for *Firefly* luciferase mRNA) RNA polymerases (Ambion Inc, Austin, Texas). mRNAs were purified using Macherey-Nagel Nucleospin® RNA Clean-up kit (Macherey-Nagel, Bethlehem, PA) prior to injections.

To test if *Eve* and *Wnt1* miRNA-31 TP phenotypes are due to an increase of translated protein, we cloned *Eve* and *Wnt1* coding sequence (CDS) in ZeroBlunt vector (Thermo Fisher Scientific, Waltham, MA) (Table S1). Plasmids were linearized with *BamHI* and *in vitro* transcribed using T7 mMessage machine kit (Ambion Inc, Austin, Texas). CDS mRNA was injected into zygotes. *Firefly* mRNA was used as a control.

### 2.3. Dual luciferase quantification

The injection solutions for the dual-luciferase assay contained 20% sterile glycerol, 2 mg/ml 10,000 MW Texas Red lysine-charged dextran, 100–200 ng/ $\mu$ l *Firefly* mRNA and 100 ng/ $\mu$ l *RLuc* mRNA (*Eve*, *Wnt1*, and *Wnt5* with wildtype [WT] or mutated seeds). 30–50 embryos were collected at the mesenchyme blastula stage (24 hpf). Dual luciferase assays were performed using the Promega Dual-Luciferase Reporter

A.



B.

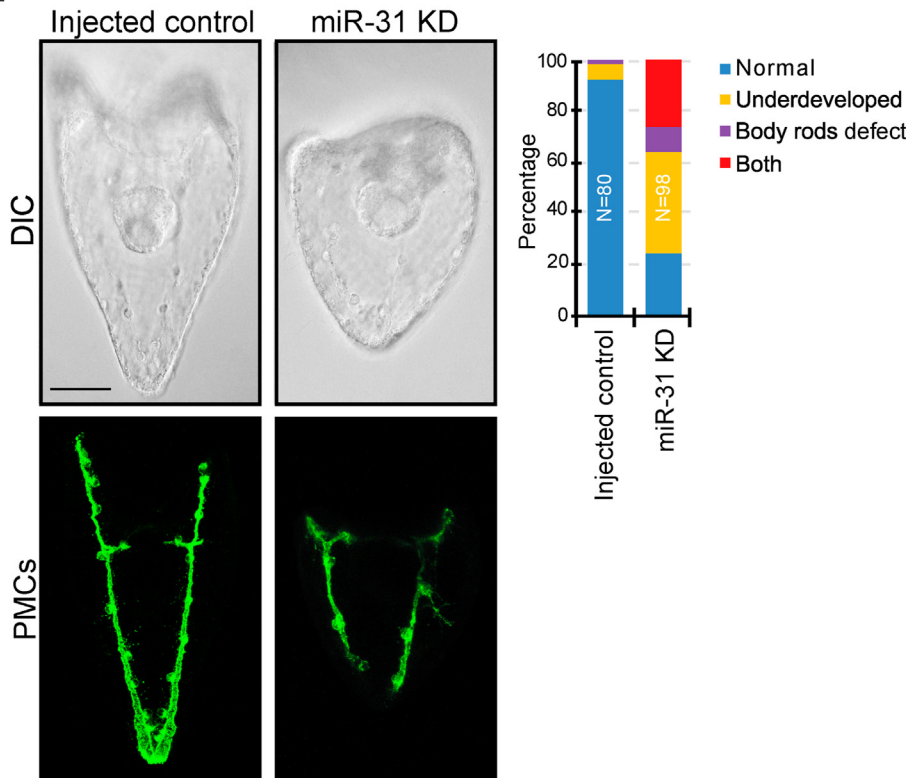


**Fig. 1. miR-31 indirectly regulates *Vegf3* expression domain and skeletogenesis by targeting *Eve*, *Wnts*, and *Fzds*.** (A) A simplified model of miR-31's indirect regulation of *Vegf3* and skeletogenesis through potential targets *Eve*, *Wnt1*, *Wnt16*, and *Fzd5/8* during mesenchyme blastula (24 hpf). Genes highlighted in yellow are potential miR-31 targets. *Eve* is activated by cWnt/ $\beta$ -catenin signaling and is expressed in both the Veg1 endoderm and ectoderm and activates *Hox11/13b* in the Veg1 endoderm (Cui et al., 2014; Peter and Davidson, 2011; Ransick et al., 2002). *Wnt1* and *Wnt16* also contribute to the activation of *Hox11/13b* in the Veg1 cells, and the positive feedback of *Hox11/13b*, *Wnt1*, and *Wnt16* occurs in Veg1 endodermal cells (Cui et al., 2014). *Wnt1* signals through *Fzd5/8* receptor to activate the ncWnt/PCP-ROCK/JNK pathway, and *Wnt16* signals through *Fzd1/2/7* to activate the ncWnt/ $Ca^{2+}$ -PKC pathway (Martínez-Bartolomé and Range, 2019; Range et al., 2013). *Wnt1*-*Fzd5/8* and *Wnt16*-*Fzd1/2/7* cross-regulate each other (Range et al., 2013). *Wnt1*-*Fzd5/8* and/or *Wnt16*-*Fzd1/2/7* signaling lead to the activation of an unidentified factor which activates transcription factor *Pax2/5/8*, leading to activation of *Vegf3* expression (McIntyre et al., 2013; Rottinger et al., 2008). *Eve*, *Hox11/13b*, *Fzd5/8* and *Fzd1/2/7* are in part regulated through autorepression, while *Wnt1* may be regulated through autoactivation (Cui et al., 2014, 2017; Range, 2018; Range et al., 2013). (B) The shorter DVC rods and aberrant PMC patterning defects observed in miR-31 KD gastrulae (Stepicheva and Song, 2015) persist into the larval stage (5dpf). A greater number of miR-31 KD larvae are underdeveloped and/or exhibit body rods that fail to meet at the posterior end of the embryo. Maximum intensity projection of Z-stack confocal images are shown. 2 biological replicates. N is the total number of larvae examined. Scale bar = 50  $\mu$ m.

(DLR™) Assay Systems with the Promega GloMax 20/20 Luminometry System (Promega, Madison, WI). The RLuc values were normalized to the Firefly signal to account for microinjection volume differences. The data from the RLuc with mutated miR-31 seeds were normalized to the RLuc with WT 3'UTR construct.

#### 2.4. Microinjections

Microinjections were performed as previously described (Cheers and Etensohn, 2004; Stepicheva and Song, 2014) with modifications. All injection solutions were prepared in a 2.5  $\mu$ l solution consisting of 0.5  $\mu$ l of 100% glycerol and 0.5  $\mu$ l of 2 mg/ml 10,000 MW neutral non-fixable

Texas Red dextran (Thermo Fisher Scientific, Waltham, MA). Approximately 1–2  $\mu$ l (pl) was injected into each newly fertilized egg based on the size of the injection bolus at about one-fifth of the egg diameter. miR-31 inhibitor (Cel-miR-72) (miRCURY LNA power inhibitor, Qiagen, Germantown, MD) was used at a 30  $\mu$ M concentration (Stepicheva and Song, 2015). Texas Red dextran was used as an injection control (Thermo Fisher Scientific, Waltham, MA). For luciferase assays, 100–200 ng of WT or mutated Rluc construct and 100–200 ng of *Firefly* luciferase as injection control was used. miRNA target protector morpholinos (TPs) were designed against validated miR-31 seed sites identified by dual-luciferase assays and their specific flanking sequences within the 3'UTRs of *Eve* and *Wnt1* (GeneTools, LLC, Philomath, OR). The injection solution of *Eve* miR-31 TP contained 3  $\mu$ M or 300  $\mu$ M of the each of the two *Eve* miR-31 TPs and 6  $\mu$ M or 600  $\mu$ M of control TP, respectively. The control TP is against human  $\beta$ -globin and does not recognize sea urchin genes (as assessed by BLASTN against the sea urchin genome). The injection solution of control TP or *Wnt1* miR-31 TP contained 30  $\mu$ M or 300  $\mu$ M of TP. The *Eve* + *Wnt1* miR-31 TP cocktail solution contained 300  $\mu$ M of *Wnt1* miR-31 TP and 300  $\mu$ M of each of the two *Eve* miR-31 TPs. The control TP contained 900  $\mu$ M of TP.

To test for specificity of miR-31 TPs, *Eve* or *Wnt1* transcripts were microinjected to examine their overexpression phenotypes. All injection solutions were prepared in a 2.5  $\mu$ l solution consisting of 0.5  $\mu$ l of 100% glycerol and 0.5  $\mu$ l of RNase-free 2 mg/ml 10,000 MW neutral non-fluorescent Texas Red dextran (Thermo Fisher Scientific, Waltham, MA) or 500 ng of mCherry mRNA. Injection solution contained 3  $\mu$ g of *Eve* mRNA or 1.5  $\mu$ g of *Wnt1* mRNA. Control mRNA consisted of 1.5–3  $\mu$ g of *Firefly* mRNA.

## 2.5. Immunofluorescence

Embryos were fixed and immunolabeled with 1D5 at 1:50, overnight to 2 days at 4 °C as previously described (McClay et al., 1983; Sampilo et al., 2018) (gift from Dr. David McClay, Duke University). This was followed by goat anti-mouse Alexa488 (Thermo Fisher Scientific, Waltham, MA) conjugated secondary antibody at 1:300 for 1 h at room temperature. Embryos were washed 3 times with PBS-Tween (0.05% Tween-20 in 1X PBS).

## 2.6. Whole mount in situ hybridization (WMISH)

Partial coding sequences of *Eve*, *Hox11/13b*, *Wnt1*, *Wnt5*, *VegfR10*, and *Vegf3* were cloned into ZeroBlunt vector (Thermo Fisher Scientific, Waltham, MA) (Stepicheva et al., 2015; Stepicheva and Song, 2015). Pax2/5/8 CDS was generated by gBlock (Integrated DNA Technologies, Coralville, Iowa) and cloned into ZeroBlunt vector (Thermo Fisher Scientific, Waltham, MA). *Wnt16* was cloned into pGEM-T Easy Vector (Martínez-Bartolomé and Range, 2019) (Gift from Dr. Ryan Range, Auburn University). *Eve*, *Hox11/13b*, *Wnt1*, *Wnt5*, *Wnt16*, *Pax2/5/8*, and *Vegf3* were linearized with restriction enzymes *EcoRI*, *BamHI*, *BamHI*, *NotI*, *BamHI*, *SpeI*, and *BamHI*, respectively, using FastDigest™ (Thermo Fisher Scientific, Waltham, MA). *Eve*, *Wnt5*, *Hox11/13b*, *Wnt1*, and *Pax2/5/8* were *in vitro* transcribed with Sp6 RNA polymerase, and *Vegf3* and *Wnt16* were *in vitro* transcribed with T7 RNA polymerase of the DIG RNA Labeling Kit (Millipore Sigma, St. Louis, MO).

## 2.7. Phenotyping

To measure the length of dorsoventral connecting rods (DVCs), ZEISS Observer Z1 microscope was used to take Z-stacks of differential interference contrast (DIC) and 1D5-immunolabeled images. N is the total number of embryos examined except where otherwise stated. ZEISS AxioCam105 color camera was used to take *in situ* images. AxioVision software was used to measure the length of DVCs, PMC migration distance, and *in situ* gene expressions. Zen 3.1 software (Carl Zeiss Microscopy, White Plains, NY) was used to determine the center of gastrulae in

vegetal views to measure angles of *Vegf3* expression domains, VE, and DE domains. Representative images were taken with Zeiss LSM 880 scanning confocal microscope using Zen software or ZEISS Observer Z1 using AxioVision software (Carl Zeiss Microscopy, LLC, White Plains, NY).

## 2.8. Real-time quantitative PCR (qPCR)

To measure the transcriptional changes of genes within our model, and biomineralization genes, we used real-time, quantitative PCR (qPCR). We injected 100 zygotes and collected them at blastulae (24 hpf) for injected control, miR-31 KD, *Eve* miR-31 TP, *Wnt1* miR-31 TP, and *Eve* + *Wnt1* miR-31 TP. Total RNA was extracted by using the Macherey-Nagel Nucleospin® RNA Isolation XS kit (Macherey-Nagel, Bethlehem, PA). cDNA was synthesized using iScript cDNA synthesis kit (Bio-Rad, Hercules, CA). qPCR was performed using 2.5 embryo equivalents for each reaction with the Fast SYBR or PowerUp Green PCR Master Mix (Thermo Fisher Scientific, Waltham, MA) in the QuantStudio 6 Real-Time PCR cyclers system (Thermo Fisher Scientific, Waltham, MA). Results were normalized to the mRNA expression of the housekeeping gene, *ubiquitin*, and shown as fold changes compared to injected control embryos using the  $\Delta\Delta$ Ct method as previously described (Stepicheva et al., 2015). Primer sequences were designed using the Primer 3 Program (Rozen and Skaletsky, 2000) and are listed in Table S1. 3–6 biological replicates were conducted.

## 3. Results

### 3.1. miR-31 indirectly regulates *Vegf3* expression and skeletogenesis

We previously found miR-31 KD embryos displayed expanded and anteriorly shifted *Vegf3* expression domain compared to the injected control (Stepicheva and Song, 2015). miR-31's regulation of *Vegf3* is likely to be indirect, since it does not contain any predicted miR-31 binding sites (Stepicheva and Song, 2015). We propose a working model based on existing literature of how miR-31 indirectly regulates *Vegf3* (Fig. 1A). In this model, *Eve* is the most upstream component of this pathway, since *Eve* controls the specification of the Veg1 lineage through its activation of *Hox11/13b* in the Veg1 endoderm at 24 hpf (Cui et al., 2014; Peter and Davidson, 2010). In addition to *Eve*, *Wnt1* and *Wnt16* also contribute to the activation of *Hox11/13b* in the Veg1 cells, and the positive feedback circuit of *Hox11/13b*, *Wnt1*, and *Wnt16* occurs in Veg1 endodermal cells (Cui et al., 2014). The receptor and signaling pathways for *Wnt1* and *Wnt16* are Fzd5/8-ROCK/JNK and Fzd1/2/7-PKC, respectively; perturbation of either Fzd5/8, ROCK, *Wnt16*, Fzd1/2/7 or PKC leads to loss of skeleton (Croce et al., 2006; Martínez-Bartolomé and Range, 2019; Range et al., 2013). It has been implicated that *Wnt16* acts downstream of *Wnt1*-Fzd5/8-JNK signaling (Martínez-Bartolomé and Range, 2019). Fzd1/2/7-PKC signaling then activates an unidentified activator of Pax2/5/8, which in turn, leads to the activation of *Vegf3*, as observed in *L. variegatus* (*Lv*) (McIntyre et al., 2013). *LvWnt5* KD results in loss of Pax2/5/8 and *Vegf3* expression in the BE-DVM, in addition to embryos lacking skeleton (McIntyre et al., 2013). This potentially indicates that *LvWnt5* regulates *Vegf3* and skeletogenesis. However, *Wnt5* KD in *S. purpuratus* (*SpWnt5*) resulted in no change in expression levels of ectodermal genes *nk1*, *sp5*, *unc4.1*, *hox7*, *lrxA*, and *msx*, except for an increase in *Wnt5* transcripts (Cui et al., 2014). This suggests that *Wnt5* may not be the ligand that specifies the BE to activate *Vegf3* in *S. purpuratus*, although this was not directly tested in this study (Cui et al., 2014). Unlike *LvWnt5*, *SpWnt5* KD had no impact on *Hox11/13b* (Cui et al., 2014; McIntyre et al., 2013). Additionally, *SpHox11/13b* KD resulted in decreased *Wnt1* and *Wnt16* but did not alter *Wnt5* levels (Cui et al., 2014). Thus, *SpWnt1* and *SpWnt16* are likely to function as the *LvWnt5* in activating genes expressed in the border ectoderm in *S. purpuratus* (Cui et al., 2014).

Within this simplified model, we bioinformatically identified potential miR-31 binding sites within the 3'UTRs of *Eve*, *Wnt1*, *Wnt5*, *Wnt16*,

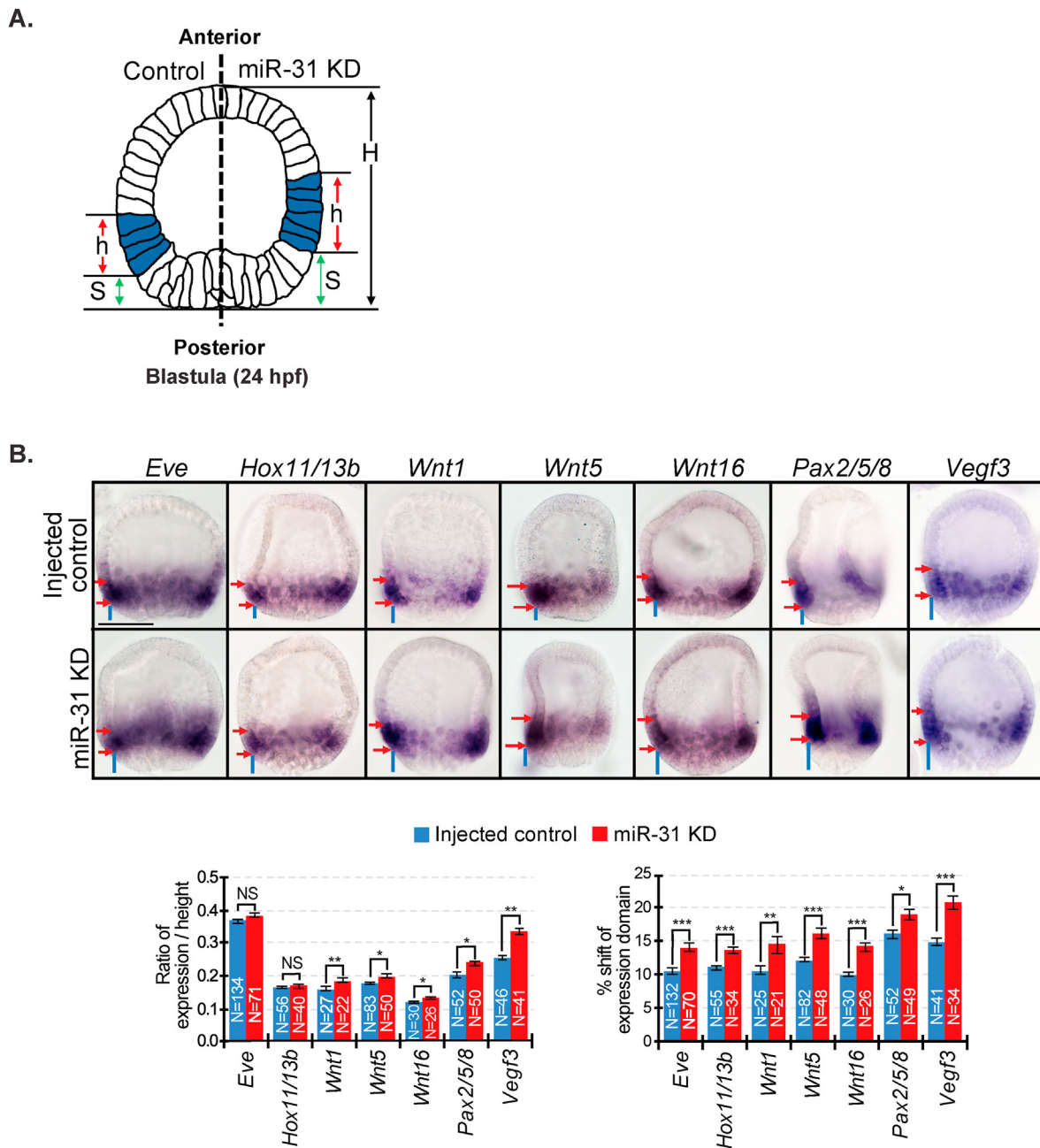


**Fig. 2.** miR-31 KD results in expansion and anterior shift of Veg1 endodermal and Veg1 ectodermal gene expression domains. (A) The spatial expression domains (h) and anterior shift (S) were measured on both sides of each embryo. The average expression domain is calculated by taking the average of the ratio of h/H from each side. The anterior shift is measured by taking the average of the ratios of S/H from each side. (B) miR-31 KD mesenchyme blastulae (24 hpf) have an anterior shift in spatial expression domain of all transcripts expressed in the Veg1 endoderm and Veg1 ectoderm compared to control. miR-31 KD embryos have expanded expression domains of *Wnt1*, *Wnt5*, *Wnt16*, *Pax2/5/8*, and *Vegf3* compared to control. Red arrows delineate expression domains. Blue lines indicate shift of expression domain. NS=Not significant, \* $p < 0.05$ , \*\* $p < 0.001$ , \*\*\* $p < 0.0001$  using Student's t-test. All error bars represent SEM. 2–3 biological replicates. Scale bar = 50  $\mu$ m.

and *Fzd5/8* transcripts (Fig. 1A). The circuitries of *Eve*, *Hox11/13b*, *Wnt1-Fzd5/8-JNK*, and *Wnt16-Fzd1/2/7-PKC* are highly auto-regulated, as well as highly cross-regulated (Cui et al., 2014, 2017; Range, 2018; Range et al., 2013). Thus, perturbing one component would be likely to alter the expression of other genes in the pathway.

Previously, miR-31 KD induced defects in gastrulae, including shortened DVCs and PMC patterning defects (Stepicheva and Song, 2015). We examined the impact of miR-31 KD in larval development and found that injected control larvae (5 days post fertilization; dpf) have an elongated pyramidal body shape, whereas miR-31 KD larvae appear

smaller and rounder (Fig. 1B). The control larvae have body rods that meet converge at the posterior end; however, miR-31 KD larvae have body rods that failed to meet at the posterior end, indicating that miR-31 KD defects are long-lasting and not recoverable (Fig. 1B).

### 3.2. Knockdown of miR-31 results in expanded and anteriorly shifted spatial expression of transcripts expressed in Veg1 cells

To understand the mechanism of miR-31's regulation of *Vegf3*, we tested the spatial expression of several transcripts in the Veg1 ectodermal

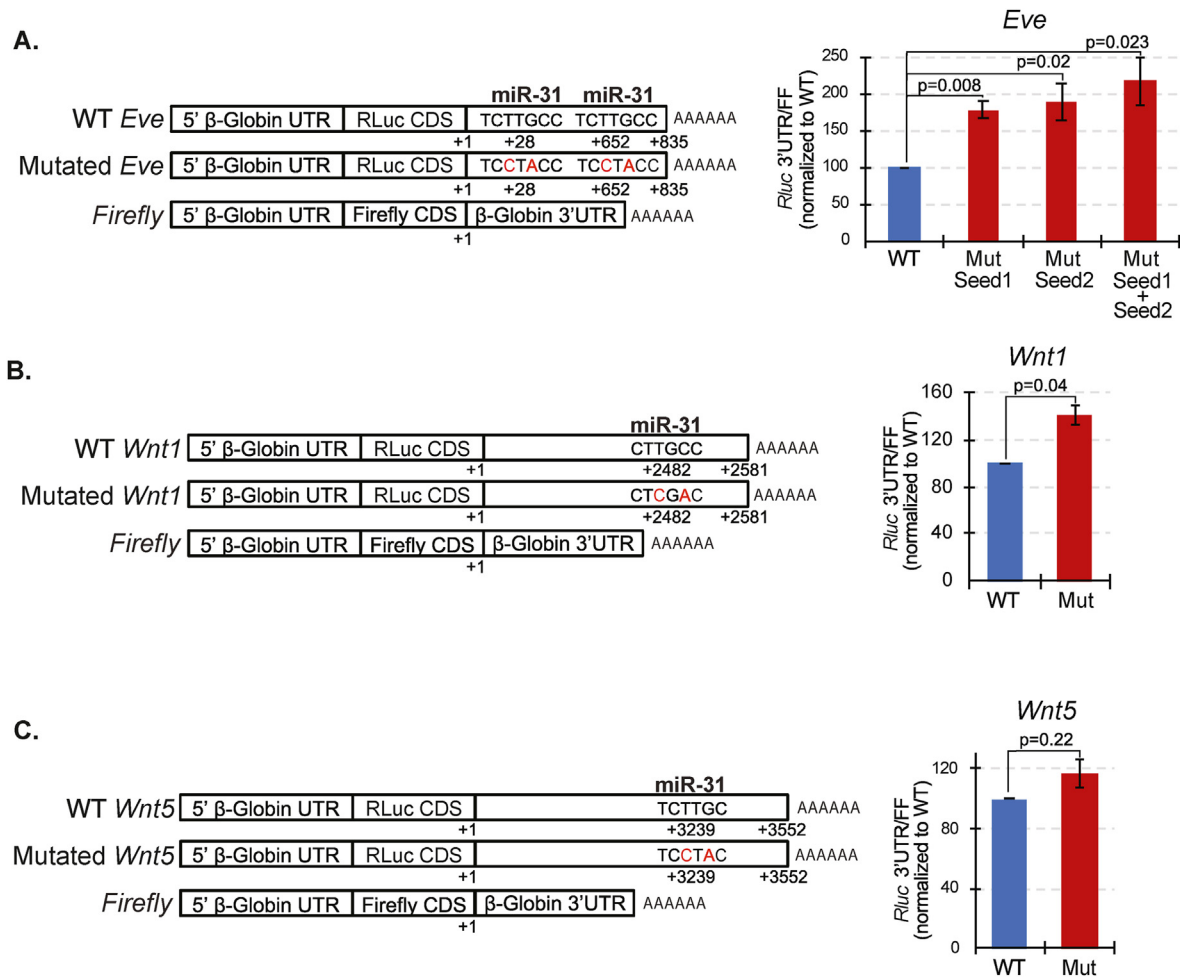


**Fig. 3. miR-31 directly suppresses *Eve* and *Wnt1*.** (A) Dual luciferase assays were conducted at mesenchyme blastula stage (24 hpf). The RLuc values were first normalized to the co-injected Firefly values. The ratios of normalized RLuc values with mutated miR-31 seed to the RLuc with WT miR-31 seed are presented. Luciferase readings of embryos injected with mutated (Mut) miR-31 3'UTR binding sites of *Eve* were increased significantly in comparison to embryos injected with the WT 3'UTRs, indicating that miR-31 directly represses *Eve*. (B) *Wnt1* has a mismatch of the first T nucleotide of the miR-31 seed sequence. *Wnt1* is directly suppressed by miR-31. (C) *Wnt5* contains a mismatch of the last C nucleotide of the miR-31 seed sequence. *Wnt5* is not directly suppressed by miR-31 or experiences weak miRNA-mRNA binding affinity. 3–4 biological replicates. P-value was analyzed using Student's t-test. All error bars represent SEM.

and endodermal cells in injected control and miR-31 KD mesenchyme blastulae at 24 hpf (Fig. 2). During this time, *Eve* and *Wnt5* are expressed in both Veg1 endoderm and Veg1 ectoderm (same as *Vegf3*), whereas *Hox11/13b*, *Wnt1*, and *Wnt16* are expressed in the Veg1 endoderm, and *Pax2/5/8* is expressed in the Veg1 ectoderm (Cui et al., 2014). In miR-31 KD blastulae, all transcripts examined have a significant anterior shift in their expression domain, and all transcripts also have an expanded expression domain (except for *Eve* and *Hox11/13b*) (Fig. 2B), similar to the anterior shift and expansion of *Vegf3* in the Veg1 endoderm and Veg1 ectoderm.

### 3.3. miR-31 directly suppresses *Eve* and *Wnt1*

Since *Vegf3* does not contain a miR-31 binding site, we bioinformatically identified potential miR-31 targets within our proposed pathway (Fig. 1A). We found that *Eve*, *Wnt1*, *Wnt16*, and *Fzd5/8* have predicted miR-31 regulatory sites within their 3'UTRs. We prioritized our analysis of *Eve*, *Wnt1* and *Wnt5* for the following reasons: *Eve* is the most upstream regulator in our model; *Wnt1* (not *Wnt16*) has a significant effect on Veg1 ectodermal gene expression that controls PMC patterning (Cui et al., 2014); and *LvWnt5* is critical for *LvVegf3* expression (McIntyre et al., 2013). To test miR-31's direct regulation of *Eve*, *Wnt1*, and *Wnt5*,

their 3'UTRs were cloned downstream of the RLuc reporter construct. RLuc with WT or mutated miR-31 binding sites were co-injected with *Firefly* reporter construct as a normalization control into newly fertilized eggs. Mutated miR-31 binding sites will abolish target recognition by endogenous miR-31, preventing miR-31's binding and regulation. *Eve* has two predicted miR-31 binding sites, and both *Wnt1* and *Wnt5* have predicted truncated miR-31 binding sites. Of the miR-31 reverse complement seed sequence (TCTTGCC), *Wnt1* has a mismatch of the first T nucleotide (nt) and *Wnt5* contains a mismatch of the last C nucleotide. miRNA binding of 6 nts that is offset by a single nucleotide can also mediate detectable repression, but are less effective than a 7–8 nt perfect match (Bartel, 2018; Jan et al., 2011; Kim et al., 2016). Non-canonical sites (imperfect seed matches) have also been found to be effective in downregulating gene expression (Khorshid et al., 2013). Dual luciferase assays (24 hpf) indicate that miR-31 directly suppresses *Eve* and *Wnt1*. *Wnt5* is not directly suppressed by miR-31, or experiences weak miR-31-mRNA binding affinity (Fig. 3). The relative change of *Wnt1* luciferase readout was not as high as *Eve* luciferase readout, potentially indicating that miR-31's binding to *Wnt1* is not as strong as its binding to *Eve*.

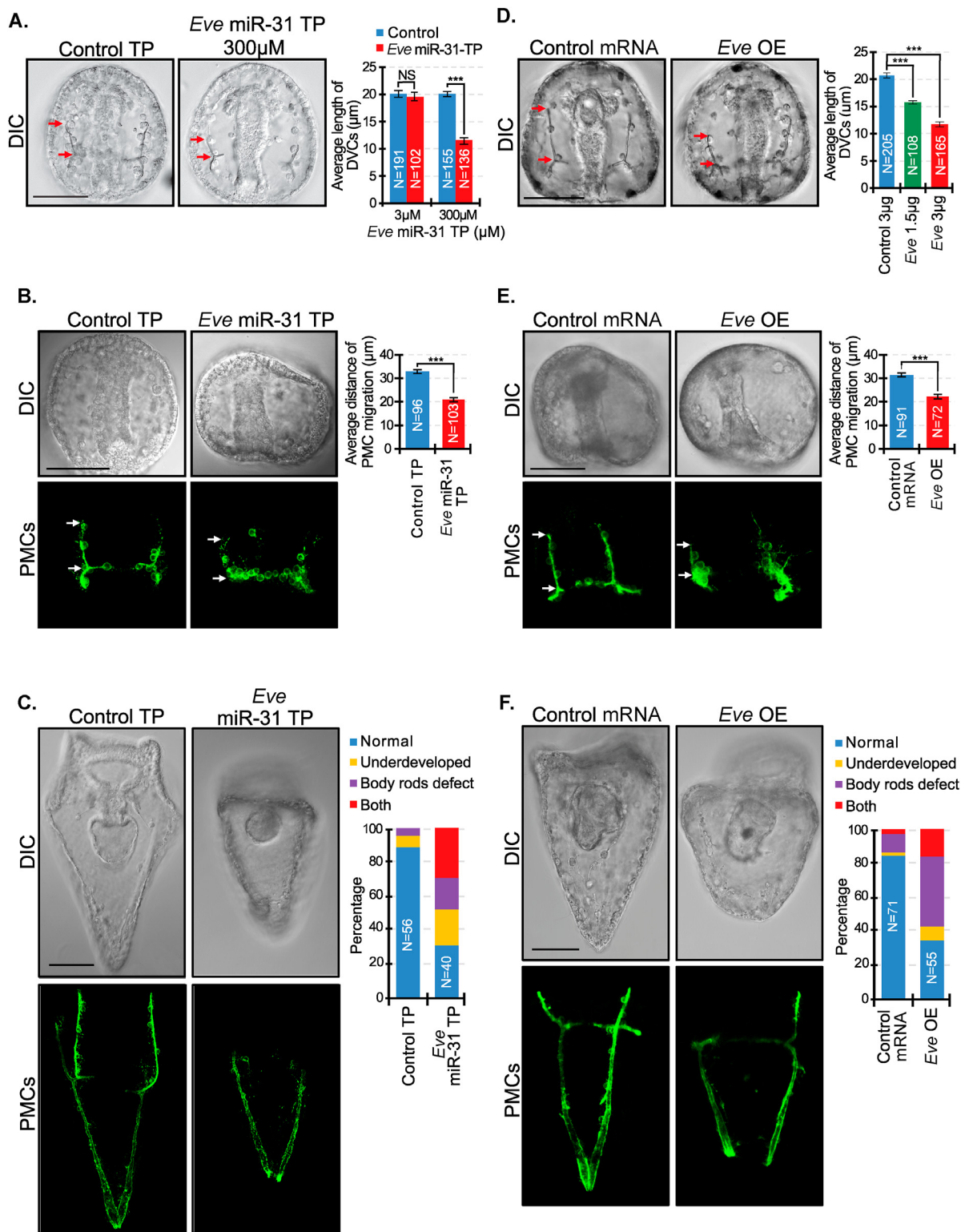


**Fig. 4. Removal of miR-31 suppression of *Eve* and *Eve* overexpression results in shortening of the DVCs and aberrant PMC patterning that persists into the larval stage.** (A) *Eve* miR-31 TP injected gastrulae (48 hpf) had decreased DVC length in a dose-dependent manner compared to the control TP. Red arrows indicate the length of DVCs. P-value was analyzed using Student's t-test. 3 biological replicates. NS = not significant. N is the total number of spicules examined. (B) Embryos were immunolabeled with PMC antibody, 1D5 (McClay et al., 1983). PMCs in *Eve* miR-31 TP injected embryos exhibit less anterior migration compared to the control injected embryos. P-value was analyzed using Student's t-test. (C) *Eve* miR-31 TP injected larval stage (5 dpf) development displayed body rods that failed to meet at the posterior end and overall greater percentage of underdeveloped larvae compared to control. 3 biological replicates. (D) Overexpression of *Eve* (3 μg or 1.5 μg total mRNA in 2.5 μl of injection stock solution) recapitulated shorter DVCs as in *Eve* miR-31 TP injected embryos in a dose-dependent manner. P-value was analyzed using Student's t-test. N is the total number of spicules examined. (E) *Eve* overexpression resulted in similar PMC anterior migration defects in *Eve* miR-31 TP gastrulae. (F) *Eve* overexpression resulted in developmental delay and body rod defects, similar to *Eve* miR-31 TP larvae. P-value was analyzed using Student's t-test. 3 biological replicates. \*\*\*p < 0.0001. All error bars represent SEM. Scale bar = 50 μm. N is the total number of embryos examined except where otherwise stated. Maximum intensity projection of Z-stack confocal images are presented for the PMC patterning.

### 3.4. Removal of miR-31 suppression of *Eve* and overexpression of *Eve* result in skeletogenic and PMC patterning defects

To test if the removal of miR-31 suppression of *Eve* had an impact in skeletogenesis, we designed miRNA TPs against the validated miR-31 seed sites (Remsburg et al., 2019; Staton and Giraldez, 2011; Stepicheva and Song, 2015). TPs are synthetic morpholino oligonucleotides designed to bind to miR-31 regulatory seed sites of its target and unique nucleotides immediately flanking the seed, blocking miR-31's regulatory function (Remsburg et al., 2019). Newly fertilized eggs were microinjected with *Eve* miR-31 TPs at two concentrations. We observed a dose-dependent 4% and 38% decrease in spicule length in 3 and 300  $\mu$ M of *Eve* miR-31 TP injected embryos compared to the control TP, respectively (Fig. 4A). Since we observed a change in spicule length, and PMCs are the only cells within the embryo that make the larval skeleton, we examined how PMC patterning is affected in *Eve* miR-31 TP injected embryos. Results indicate that *Eve* miR-31 TP gastrulae PMCs exhibited less anterior migration than the PMCs in control TP embryos (Fig. 4B). We also observed that *Eve* miR-31 TP injected larvae (5 dpf) appear smaller in size with body rods that often failed to converge at the posterior end compared to the control TP (Fig. 4C).

To test the role of miR-31's direct post-transcriptional suppression of *Eve*, we examined if overexpression of *Eve* would result in similar phenotypes as *Eve* miR-31 TP, supporting the role of miR-31 in repressing *Eve* protein levels. We cloned and injected *Eve* CDS transcripts into newly fertilized eggs. Results indicate that overall *Eve* overexpression (OE) phenotypes mimicked that of *Eve* miR-31 TP injected embryos (Fig. 4D–F). *Eve* OE resulted in the dose-dependent shortening of DVCs and decreased PMC anterior migration compared to control (Fig. 4D and E). *Eve* OE also led to smaller larvae with body rods that failed to meet at the posterior end, similar to defects observed in *Eve* miR-31 TP, indicating that an increase in *Eve* impacts skeletogenesis and PMC patterning (Fig. 4).

### 3.5. Removal of miR-31 suppression of *Wnt1* results in shorter DVCs, while *Wnt1* overexpression results in supernumerary skeletal rudiments and exogastrulation

Since we found miR-31 directly suppresses *Wnt1* (Fig. 3), we examined how the removal of miR-31 suppression of *Wnt1* impacts skeletogenesis and PMC patterning. We microinjected newly fertilized eggs with *Wnt1* miR-31 TP to specifically block miR-31's binding within the *Wnt1* 3'UTR. We observed a dose-dependent decrease in DVC length in *Wnt1* miR-31 TP injected embryos compared to control TP embryos (Fig. 5A). PMC patterning in *Wnt1* miR-31 TP (300  $\mu$ M) injected gastrulae at first glance displayed no apparent defects. However, measurements of the distance of their anterior migration revealed that the PMCs in *Wnt1* miR-31 TP injected gastrulae did not migrate as far anteriorly, compared to the PMCs in control TP injected gastrulae (Fig. 5B). *Wnt1* miR-31 TP injected larvae (5 dpf) exhibited body rods that failed to meet at the posterior end which may contribute to the rounded body appearance, as opposed to control TP larvae with body rods that meet at the posterior end, giving the larvae a pyramidal body shape (Fig. 5C). These are similar to defects observed in *Eve* miR-31 TP and *Eve* CDS injected larvae (Fig. 4C, F), suggesting that *Eve* and *Wnt1* are likely to regulate a similar pathway that controls proper body rod formation.

To mimic the effect of *Wnt1* miR-31 TP where *Wnt1* translation would be increased, we cloned and injected *Wnt1* CDS transcripts (1.5  $\mu$ g/ $\mu$ l) into newly fertilized eggs. We observed that *Wnt1* OE resulted in gastrulae with supernumerary skeletal tri-radiate rudiments (25%), exogastrulation (22%), widened gut (9%), or a combination of these phenotypes (19%) (Fig. 5D). In *Wnt1* OE embryos with normal two spicule tri-radiates, the length of their DVCs was significantly shorter compared to control mRNA injected embryos. *Wnt1* OE embryos did not survive well past the gastrula stage, with approximately 50% of the abnormal embryos undergoing exogastrulation (Fig. 5D). Higher

concentrations (3  $\mu$ g/ $\mu$ l) resulted in embryonic lethality.

### 3.6. Removal of miR-31 suppression of both *Eve* and *Wnt1* recapitulates skeletal and PMC patterning defects observed in miR-31 KD embryos

To examine the impact of blocking miR-31's suppression of both *Eve* and *Wnt1*, we microinjected a cocktail of *Eve* miR-31 TPs and *Wnt1* miR-31 TP into newly fertilized eggs. We observed a significant decrease in the length of DVCs (Fig. 6A). *Eve* and *Wnt1* miR-31 TP injected gastrulae also have more severe PMC patterning defects compared to the control TP, as well as compared to single *Eve* or *Wnt1* miR-31 TP injections. Phenotypes observed in the *Eve* + *Wnt1* miR-31 TP injected embryos were reminiscent of PMC anterior migration patterning defects observed in miR-31 KD embryos (Figs. 1B, 6B and 6C) (Stepicheva and Song, 2015). *Eve* + *Wnt1* miR-31 TP injected larvae also exhibited body rods that failed to meet at the posterior end, similar to miR-31 KD larvae (Fig. 1B). These results suggest that miR-31's regulation of *Eve* and *Wnt1* contributes to the miR-31 KD induced defects.

### 3.7. miR-31's direct suppression of *Eve* regulates the increased spatial expression of *Veg1* endodermal and ectodermal transcripts, and its direct suppression of *Wnt1* regulates the anterior shift of gene expression

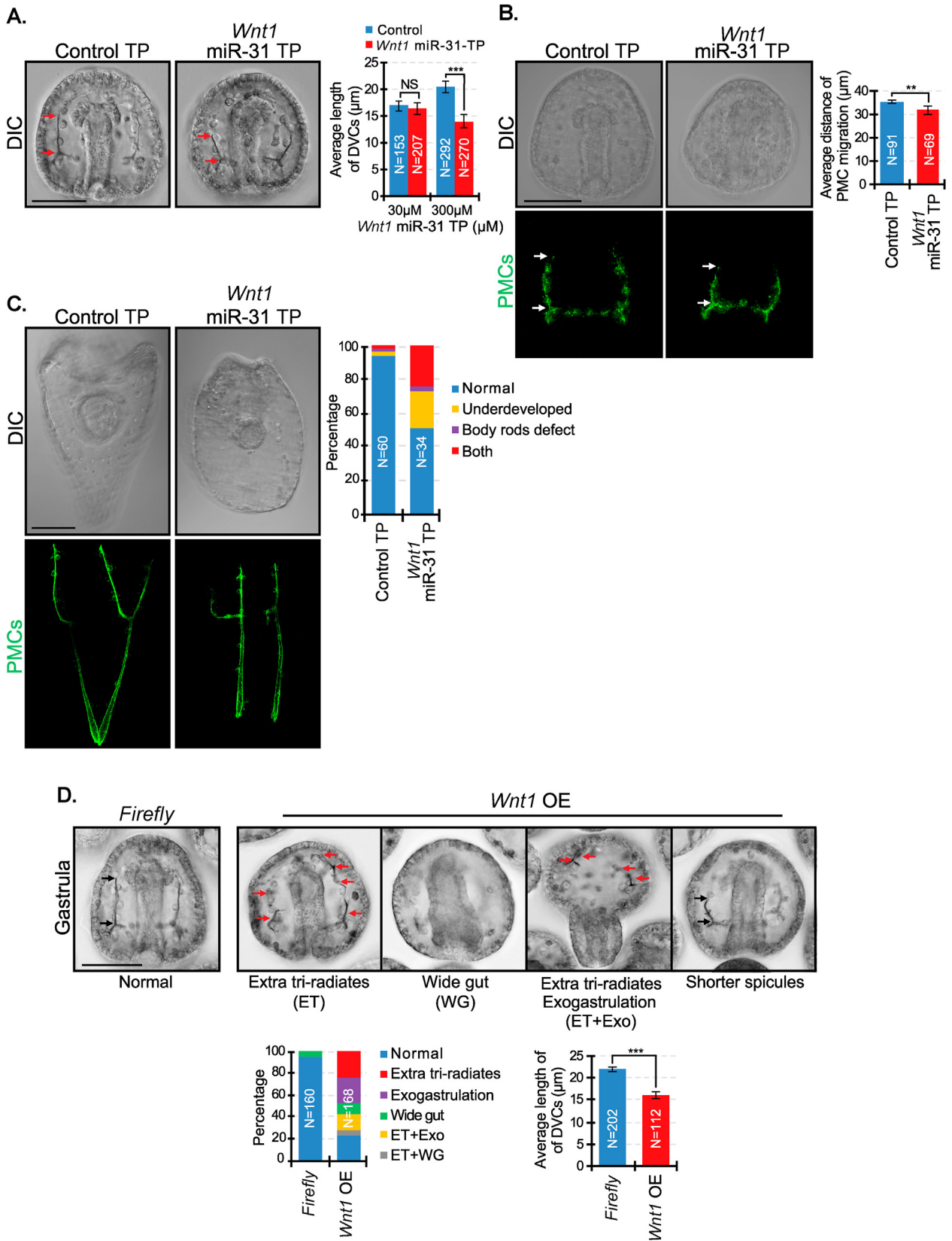
To examine the impact of blocking miR-31's direct suppression of *Eve* on expressions of genes in the proposed regulatory pathway (Fig. 1A), we microinjected *Eve* miR-31 TPs and examined the spatial expression of *Eve*, *Hox11/13b*, *Wnt1*, *Wnt5*, *Wnt16*, *Pax2/5/8*, and *Vegf3* (Fig. 7A). All their expression domains were significantly expanded, except for *Wnt16*. However, all the transcripts examined did not have an anterior shift in gene expression as observed in miR-31 KD embryos. Of note is that *Eve* OE had similar expansion of expression domain of *Vegf3* but did not cause its anterior shift in expression. (Fig. S1). Thus, while the expansion of *Vegf3* expression domain in miR-31 KD embryos may be regulated by miR-31's direct suppression of *Eve*, the anterior shift in gene expression of *Vegf3* observed in miR-31 KD is not due to this regulation.

To test if miR-31's direct regulation of *Wnt1* results in the anterior shift in the *Vegf3* expression domain in miR-31 KD embryos (Fig. 2B), we microinjected *Wnt1* miR-31 TP to block miR-31's specific binding within the *Wnt1* 3'UTR. We examined the spatial expression of *Eve*, *Wnt1*, *Wnt5*, *Wnt16*, *Pax2/5/8* and *Vegf3* in *Wnt1* miR-31 TP injected embryos in the blastula stage at 24 hpf (Fig. 7B). The expression domains of *Wnt1*, *Wnt5*, and *Wnt16* expanded compared to control TP. Importantly, an anterior shift in gene expression domain was observed for all transcripts expressed the *Veg1* endoderm and *Veg1* ectoderm, including *Vegf3* (Fig. 7B).

To test the impact of removing miR-31's direct regulation of both *Eve* and *Wnt1*, we microinjected both *Eve* and *Wnt1* miR-31 TPs and tested for gene expression domains of *Eve*, *Wnt1*, and *Vegf3*. Results indicated that the spatial expression of *Eve*, *Wnt1*, and *Vegf3* were all anteriorly shifted in their expression domains, but only *Wnt1* and *Vegf3* expression domains expanded (Fig. 7C), similar to that observed in miR-31 KD blastulae (Fig. 2).

### 3.8. Inhibition of miR-31 and removal of miR-31's suppression of *Eve* and/or *Wnt1* result in decreased levels of biomineralization transcripts compared to the control

To identify the underlying molecular mechanism that led to skeletal defects, we examined the relative expression levels of biomineralization genes, such as *P16*, *P19*, *p58A*, *SM29*, *SM37*, *SM49*, *SM50* (Adomako-Ankomah and Etensohn, 2011; Cheers and Etensohn, 2005; Livingston et al., 2006; Veis, 2011); PMC-specific cell surface protein, *Msp130* (Leaf et al., 1987); and *Otop2L*, that may play a role in regulating cytosolic calcium levels in response to extracellular signals (Hughes et al., 2004; Hurler et al., 2003; Rafiq et al., 2014; Söllner et al., 2004). All these genes are highly expressed in the PMC ventrolateral clusters that give rise



(caption on next page)

**Fig. 5. Removal of miR-31 suppression of *Wnt1* results in shorter DVC length while *Wnt1* overexpression results in supernumerary skeletal rudiments and exogastrulation.** (A) *Wnt1* miR-31 TP injected gastrulae (48 hpf) had decreased DVC length in a dose-dependent manner. Red arrows indicate the length of DVCs. P-value was analyzed using Student's t-test. 2–3 biological replicates. NS = not significant. N is the total number of spicules examined. (B) Embryos were immunolabeled with PMC antibody, 1D5. PMC anterior migration is decreased in *Wnt1* miR-31 TP injected embryos compared to the control injected embryos. P-value was analyzed using Student's t-test. 2 biological replicates. White arrows indicate PMC migration distance. (C) *Wnt1* miR-31 TP injected larvae (5dpf) appeared rounder with body rods that failed to meet at the posterior end compared to the control TP. 2 biological replicates. Maximum intensity projection of Z-stack confocal images are presented for the PMC patterning. (D) Overexpression of *Wnt1* CDS resulted in multiple developmental defects. Red arrows indicate skeletal tri-radiates. Black arrows indicate the length of DVCs. P-value was analyzed using Student's t-test. 4 biological replicates. N is the total number of spicules examined. Tri-radiates were counted through a series of Z-stack images. \*\*p < 0.001, \*\*\*p < 0.0001. All error bars represent SEM. Scale bar = 50 μm. N is the total number of embryos examined except where otherwise stated.

to the tri-radiate skeletal primordium, and in the PMCs at the tips of the larval body rods (with the exception of *SM49*) (McIntyre et al., 2014; Sun and Etensohn, 2014). Results indicate that all perturbed embryos had decreased expression of biomineralization transcripts compared to the control TP (Fig. 8). No significant change was observed for *P16* and *Otop2L* in any condition. miR-31 KD resulted in at least a 2-fold decrease in expression of *P19*, *SM29*, *SM49*, *SM50*, and *Msp130*. *Msp130* is also decreased 2-3-fold in *Wnt1* miR-31 TP and *Eve* + *Wnt1* miR-31 TP injected embryos. All *Eve* miR-31 TP injected embryos had negligible average changes (less than 2-fold) compared to the controls, except for *SM37*. In contrast, *Wnt1* miR-31-TP injected embryos had the strongest repressive effects on a number of transcripts, including *p58A*, *SM29*, *SM37*, *SM49*, *SM50* and *Msp130*. Interestingly, the combination of *Eve* and *Wnt1* miR-31 TPs seems to rescue the *Wnt1* miR-31 TP effect on gene expression of several transcripts (*p58A*, *SM29*, *SM50*, and *Msp130*), suggesting that the effects of miR-31 on *Eve* and *Wnt1* may have distinct

and inverse impacts on the expression of these genes.

**3.9. miR-31 inhibitor injected embryos have delayed PMC ingress and an ectopic *Vegf3* expression domain that correlates with PMC migration patterning defects**

To elucidate how miR-31 KD affects PMC ingress and migration patterning defects, we examined the expression of *Vegfr10* and *Vegf3* and directed migration of PMCs during different developmental time points (Fig. 9). *Vegfr10* is the presumed receptor that responds to *Vegf3* ligand and is expressed exclusively in all PMCs (Duloquin et al., 2007; Etensohn and Adomako-Ankomah, 2019). We used the *Vegfr10* RNA probe to identify PMCs that underwent epithelial to mesenchymal transition (EMT) between 18 and 26 hpf (Fig. 9A) (Katow, 2015; Rizzo et al., 2006). Typically, while undergoing epithelial to mesenchymal transition (EMT), PMCs must loosen apical junctions to their neighbors, change shape, and

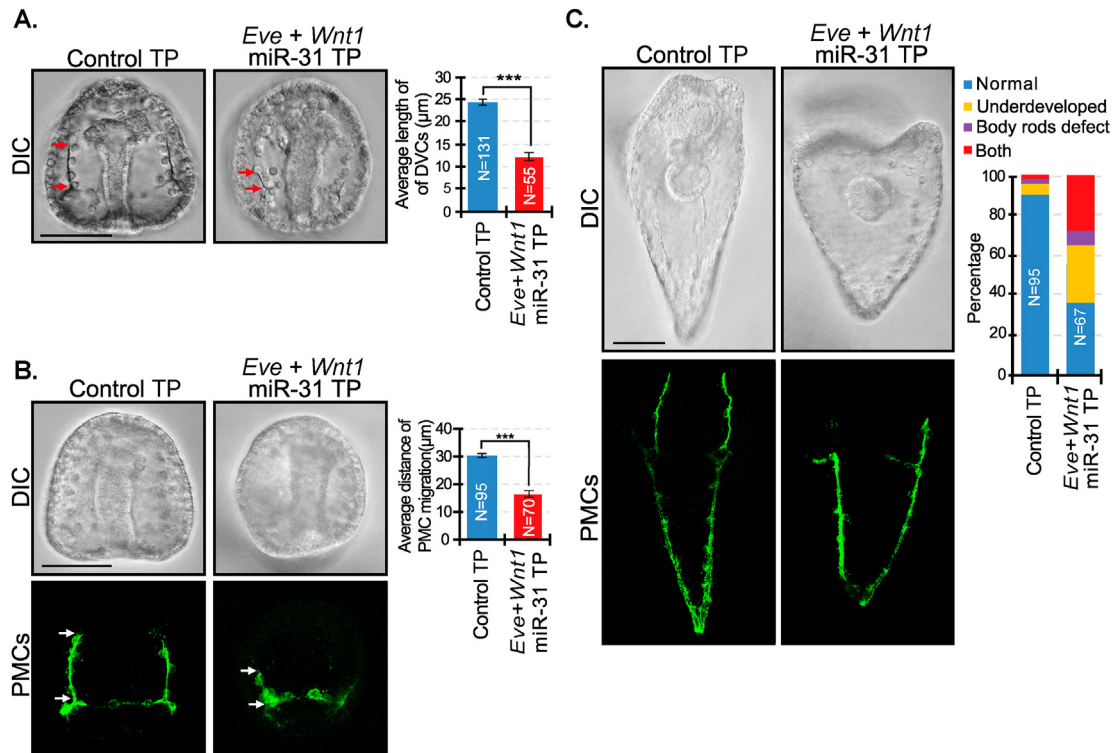


**Fig. 6. Removal of miR-31 suppression of both *Eve* and *Wnt1* results in similar skeletal and PMC patterning defects as miR-31 KD embryos.** (A) A combination of *Eve* miR-31 TP and *Wnt1* miR-31 TP resulted in a significant decrease in length of the DVCs compared to control TP gastrulae. Red arrows indicate the length of DVCs. P-value was analyzed using Student's t-test. 2 biological replicates. N is the total number of spicules examined. (B) *Eve* + *Wnt1* miR-31 TP injected embryos displayed severe anterior migration defects of PMCs compared to the control, reminiscent of defects observed in miR-31 KD gastrulae (Stepicheva and Song, 2015). P-value was analyzed using Student's t-test. 3 biological replicates. (C) Compared to the control, *Eve* + *Wnt1* miR-31 TP injected larvae (5 dpf) are smaller and have body rods that failed to meet at the posterior end, similar to miR-31 KD larvae. 3 biological replicates. \*\*\*p < 0.0001. All error bars represent SEM. Scale bar = 50 μm. N is the total number of embryos examined except where otherwise stated. Maximum intensity projection of Z-stack confocal images are shown.

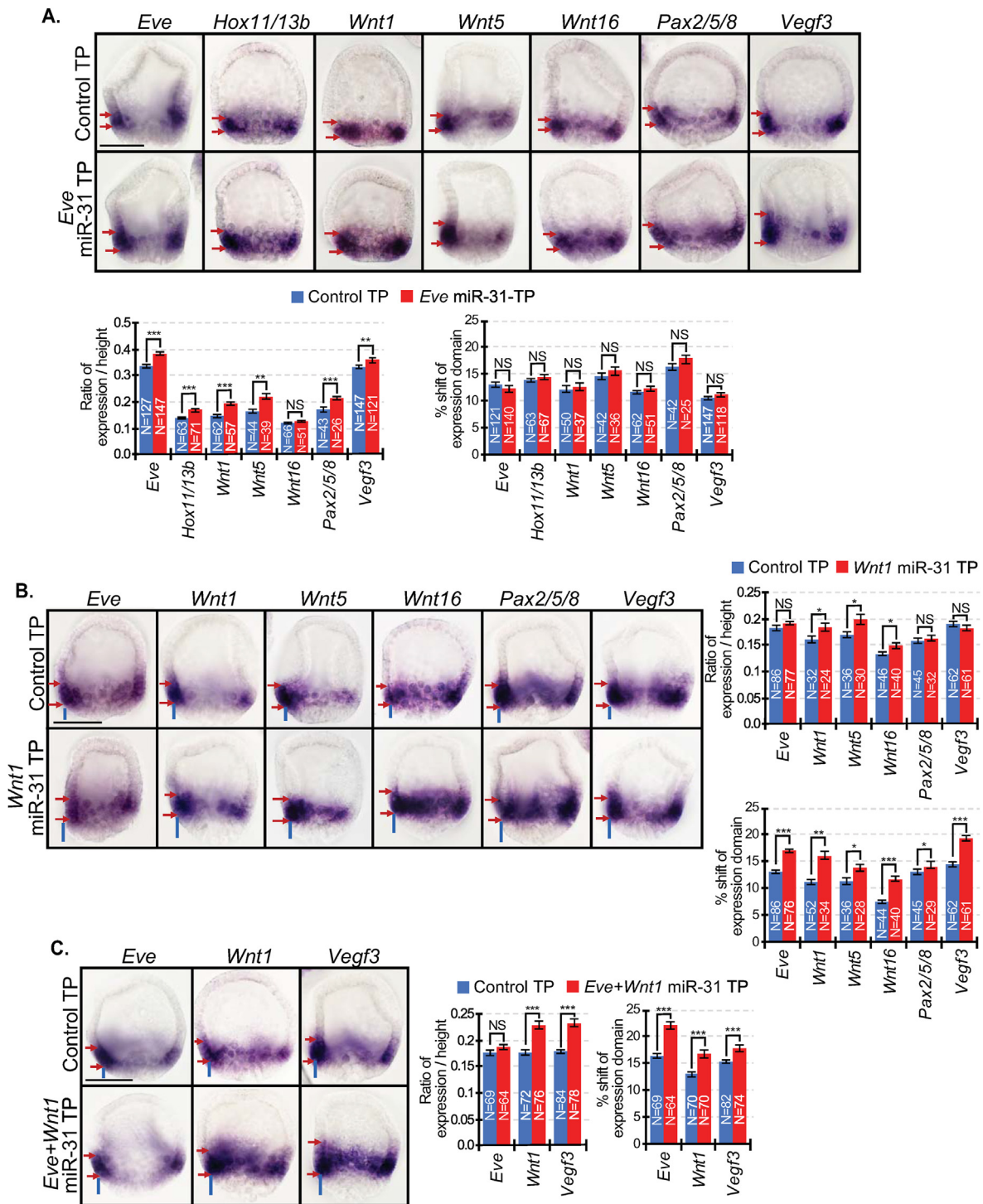


**Fig. 7. miR-31's direct suppression of *Eve* regulates the increased spatial expression of *Veg1* endodermal and ectodermal transcripts, and its direct suppression of *Wnt1* regulates the anterior shift of gene expression.** (A) In *Eve* miR-31 TP injected embryos, expression domains of all examined transcripts were significantly expanded with the exception of *Wnt16*. Red arrows delineate expression domains. (B) In *Wnt1* miR-31 TP injected embryos, the expression domains of *Wnt5* and *Wnt16* were expanded compared to control TP. An anterior shift of gene expression domain was observed for all genes. Presence of blue lines indicates a shift of expression domain. (C) *Eve* + *Wnt1* miR-31 TP injected embryos resulted in an anterior shift of the expression domains of *Vegf3*, *Eve*, and *Wnt1*. The expression domains of these transcripts also expanded, similar to that observed in miR-31 KD embryos. NS = not significant. \**p* < 0.05, \*\**p* < 0.001, \*\*\**p* < 0.0001 using Student's t-test. All error bars represent SEM. 2–4 biological replicates. Scale bar = 50  $\mu$ m. N is the total number of embryos examined.

breach the basal lamina to ingress into the blastocoel, giving these cells a 'bottle-shape'; on the other hand, cells that have completed EMT have round cell shape (Anstrom, 1992; Ettensohn, 1999; Fink and McClay, 1985; Katow and Solursh, 1981; Lyons et al., 2012; Nakajima and Burke,

1996). This includes non-skeletogenic mesenchyme cells (NSMs) and PMCs. Using the cell shape as a criterion for EMT, we have documented the number of *VegfR10*-expressing PMCs that are fully ingressed (round in cell shape) and PMCs that are undergoing ingression (bottle cell

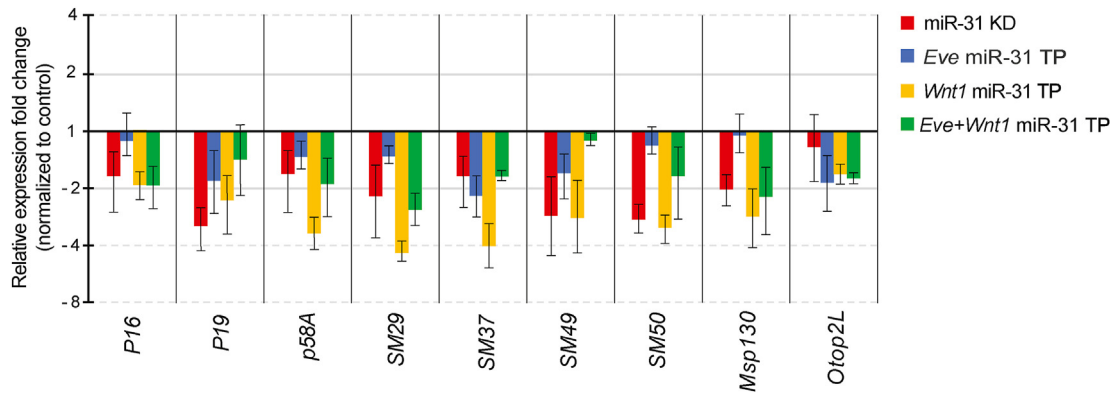


**Fig. 8. miR-31 KD, *Eve* miR-31 TP, *Wnt1* miR-31 TP, and *Eve* + *Wnt1* miR-31 TP injected embryos have decreased levels of biomineralization transcripts.** qPCR was used to measure the transcriptional changes of biomineralization and PMC genes *P16*, *P19*, *p58A*, *SM29*, *SM37*, *SM49*, *SM50*, *Msp130* and *Otop2L*. All perturbed embryos have decreased expression of biomineralization transcripts compared to the control. miR-31 KD resulted in a  $\geq 2$ -fold decrease in *P19*, *SM29*, *SM49*, *SM50*, and *Msp130*. All *Eve* miR-31 TP embryos have negligible average changes ( $< 2$ -fold) compared to the controls, except for *SM37*. In contrast, *Wnt1* miR-31 TP injected embryos have the strongest effects, resulting in more than a 2-fold decrease in *p58A*, *SM29*, *SM37*, *SM49*, *SM50* and *Msp130*. Embryos were collected at mesenchyme blastula stage (24 hpf). All error bars represent SEM. 3–5 biological replicates.

shaped) in control and miR-31 KD embryos in this series of time course experiment. In injected control blastulae, by 24 hpf, over 90% of PMCs have ingressed (Fig. 9A). In contrast, in miR-31 KD embryos at 24 hpf, only 50% of PMCs have ingressed. In fact, 30% of *VegfR10*-positive, bottled-shaped PMCs were still undergoing EMT at 26 hpf in miR-31 KD embryos, when nearly 100% of all PMCs in control embryos have fully ingressed. This delay in PMC ingression observed in miR-31 KD embryos was consistent throughout all times points examined and is unlikely due to transient delay caused by microinjections.

To test if a change in *Vegf3* expression could explain PMC patterning defects, we examined *Vegf3* expression and anterior migration of PMCs during various stages of gastrulation (32–48 hpf). We observed an interesting trend of *Vegf3* expression that correlates with anterior migration of PMCs. At 24 hpf, the anterior-posterior expression domain of *Vegf3* is significantly expanded in the miR-31 KD blastulae compared to the control (Stepicheva and Song, 2015) (Figs. 2B and 9B). However, from 40 to 48 hpf, when PMCs undergo anterior migration (Duloquin et al., 2007; Ettensohn and McClay, 1986; McIntyre et al., 2014), the expression domain of *Vegf3* in the AP region remains unchanged and is decreased in miR-31 KD gastrulae compared to the control. The decreased *Vegf3* expression domain in the miR-31 KD gastrulae correlates with their decreased anterior migration distance of PMCs, compared to the control. Further, in control gastrulae, *Vegf3* is expressed along the AP axis of the ectoderm in a gradient that likely guides the PMCs to migrate toward the anterior pole of the embryo (Fig. 9B) (Adomako-Ankomah and Ettensohn, 2013; Duloquin et al., 2007). In contrast, miR-31 KD gastrulae express concentrated *Vegf3* at the junction of the BE-DVM, but seem to lack a *Vegf3* gradient along the AP axis (Fig. 9B). At the same time that the expression of *Vegf3* along the AP axis ceases to expand and stays unchanged in the miR-31 KD embryos (40–48 hpf), the expression domain of *Vegf3* expands in the DV axis (Fig. 9C). To determine if *Vegf3*'s expression domain expands into the dorsal or ventral ectoderm, we measured the angles of these domains in between the *Vegf3* expressing BE-DVM areas. The measured angle of the ventral ectoderm is significantly narrower in miR-31 KD gastrulae compared to control gastrulae, while the angle of dorsal ectoderm remains unchanged (Fig. 9C). This result indicates that the DV expression domain of *Vegf3* in miR-31 KD gastrulae likely expands into the ventral ectoderm.

#### 4. Discussion

This study identifies that miR-31 directly post-transcriptionally represses the transcriptional factor *Eve* and the signaling ligand, *Wnt1*, in the endodermal and ectodermal gene regulatory network. Regulation

mediated by miR-31 ensures proper skeletogenesis and PMC patterning through *Vegf* signaling. Blocking miR-31's suppression of *Eve* and *Wnt1* recapitulates miR-31 KD phenotypes, indicating that miR-31 regulates skeletogenesis and PMC patterning in part through its regulation of these two RNA targets. Specifically, we found miR-31's suppression of *Eve* is responsible for the anterior expansion of *Veg1* endodermal and ectodermal transcripts; and its direct suppression of *Wnt1* regulates the anterior shift in gene expression in these domains. We also found that miR-31's indirect regulation of *Vegf3* impacts the anterior migration of PMCs. Overall, this work provides a better understanding of the molecular mechanism of how miR-31 regulates *Vegf3* expression to regulate skeletogenesis and PMC patterning.

Since we observed aberrant *Vegf3* spatial expression in miR-31 KD embryos (Stepicheva and Song, 2015), we examined the molecular impact of miR-31 on genes expressed in the same cells as *Vegf3* (*Veg1* endoderm and *Veg1* ectoderm), focusing on genes in our proposed pathway (Fig. 1A). Results indicate that all genes tested, except for *Eve* and *Hox11/13b*, had expanded expression domains at 24 hpf (Fig. 2B). Interestingly, when miR-31 inhibitor was injected at a lower concentration (20  $\mu$ M), *Eve* expression domain was significantly expanded (Fig. S2). Since *Eve* and *Hox11/13b* are autoregulated by negative feedback, an increase of *Eve* or *Hox11/13b* protein may result in repression of its own transcription (Cui et al., 2014, 2017). It is possible that a higher concentration of injected miR-31 inhibitor (30  $\mu$ M) led to sufficient increase of translated *Eve* that induces autorepression of its own transcription. However, increased *Eve* protein may still act as an activator for target genes before autorepression is induced.

We also observed that in miR-31 KD blastulae, *Wnt1*, *Wnt5*, *Wnt16*, and *Pax2/5/8* expression domain expanded compared to the injected control (Fig. 2B). *Eve* and *Wnt1* are both activators of *Wnt5* (Cui et al., 2014). Our results identified that miR-31 directly suppresses *Eve* and *Wnt1*, but not *Wnt5* (Fig. 3). Removing miR-31's suppression of *Eve* and *Wnt1* may activate transcription of *Wnt5*. miR-31 KD may lead to increased translated *Wnt1*, which may autoactivate its own transcription (Cui et al., 2014). This increase in *Wnt1* may also explain the expanded expression of *Wnt16*, since *Wnt1* activates *Wnt16* (Cui et al., 2014). We speculate that the increased expression of *Pax2/5/8* in miR-31 KD embryos may result from increased *Wnt1* and *Wnt16*. The expanded expression of *Pax2/5/8* in the BE may, in turn, lead to increased expression of *Vegf3* (Rottinger et al., 2008). Many of the genes in this proposed pathway are autoregulated; for example, *Hox11/13b*, *Eve*, *Fzd5/8* and *Fzd1/2/7* are autorepressive, while *Wnt1* can activate its own transcription (Cui et al., 2014, 2017; Range, 2018; Range et al., 2013). Additionally, each of the components in the pathway is also

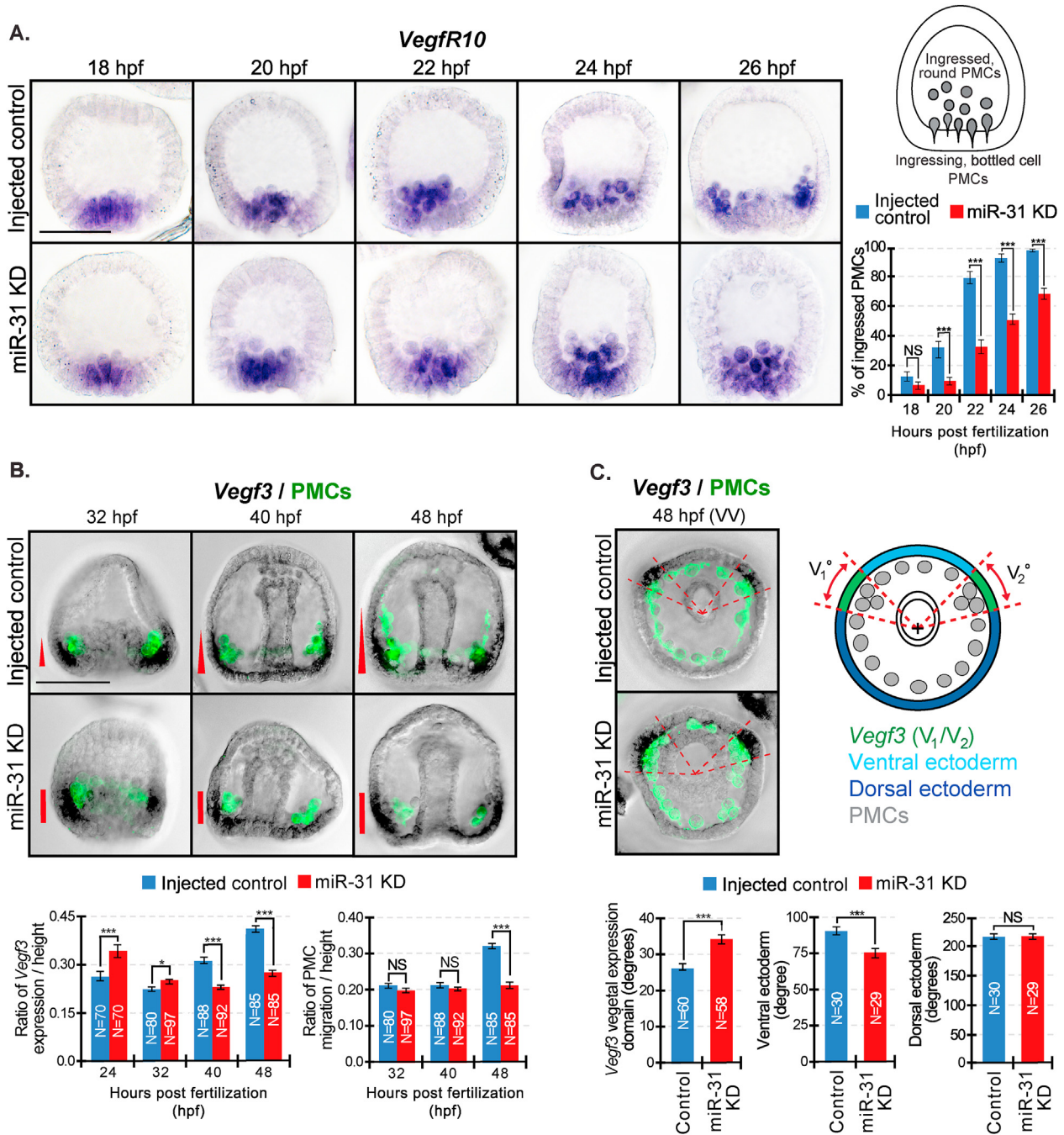


**Fig. 9. miR-31 KD embryos exhibit a delay in PMC ingression and express ectopic *Vegf3* expression domain that correlates with PMC patterning defects.** (A) Control and miR-31 KD embryos were collected at various time points spanning PMC ingression. *VegfR10*-expressing PMCs were categorized as either “ingressed, round” PMCs or “ingressing, bottle cell” PMCs. *VegfR10*-positive PMCs were counted through a series of Z-stack images. The percentage of “ingressed, round” PMCs from each embryo were calculated from the total of *VegfR10*-expressing PMCs. Average percentage was taken from each time point. For all conditions, a total of 30 embryos were measured for 3 biological replicates. NS = not significant, \*\*\* $p < 0.0001$  using Cochran-Mantel-Haenszel test. All error bars represent SEM. 3 biological replicates. Scale bar = 50  $\mu$ m. (B) Embryos undergoing gastrulation were collected between 32 and 48 hpf. Embryos were first hybridized with *Vegf3* RNA probe and followed with immunolabeling against 1D5 antibody that recognizes the PMCs (McClay et al., 1983). In control gastrulae, PMCs have migrated anteriorly in parallel to the *Vegf3* gradient at 48hpf. In miR-31 KD gastrulae at 48 hpf, PMCs are clustered next to the concentrated *Vegf3* expression domain. The general trend of *Vegf3* expression domain correlates with the anterior distance of PMC migration. (C) *Vegf3* expression is indicated in red. Zen software was used to determine the center of gastrulae in the vegetal view and to determine angles of *Vegf3* expression, VE, and DE domains. In the vegetal view (VV), the measured angle of *Vegf3* ( $V_1/V_2$ ) expression domain in miR-31 KD is expanded into the VE compared to control. N is the total number of *Vegf3* expression domains measured. 3 biological replicates. NS = not significant. \* $p < 0.05$ , \*\*\* $p < 0.0001$  using Student’s t-test. All error bars represent SEM. Scale bar = 50  $\mu$ m. Representative images were taken with ZEISS Observer Z1 microscope.

potentially cross-regulating each other (Fig. 1A).

We observed that removing miR-31's direct suppression of *Eve* resulted in decreased spicule length and abnormally clustered PMCs (Fig. 4A and B). These defects persisted into the larval stage, where *Eve* miR-31 TP larvae appeared smaller in size with body rods that often failed to meet at the posterior end (Fig. 4C). These phenotypes are similar but less severe than those observed in miR-31 KD embryos (Stepicheva and Song, 2015). In *Eve* miR-31 TP embryos, we also observed an expanded *Eve* expression domain, indicating that the level of translated *Eve* may not be high enough to autorepress its own transcription (Fig. 7A). Additionally, *Eve* miR-31 TP resulted in an expansion of *Vegf3* and all transcripts of genes proposed to be upstream of *Vegf3* and downstream of *Eve* within our model, with the exception of *Wnt16* (Figs. 1A and 7A).

As a control for *Eve* miR-31 TP and to test that PMC defects observed are due to increased translated *Eve*, we injected *Eve* CDS transcripts into zygotes. Similar to miR-31 KD (Stepicheva and Song, 2015) and *Eve* miR-31 TP embryos (Fig. 4A–C), *Eve* OE embryos had PMC defects that persisted into the larval stage (5dpf), indicating that *Eve* regulates skeletogenesis and PMC patterning (Figs. 1B, 4C and 4F). Removing miR-31's suppression of *Eve* is sufficient to cause increased translation of *Eve*, which increases *Vegf3* expression. This is demonstrated by *Eve* OE blastulae, which exhibit an increased and expanded *Vegf3* expression, similar to miR-31 KD and *Eve* miR-31 TP blastulae (Fig. S1). In embryos injected with the lower concentration of miR-31 KD (20  $\mu$ M) (Fig. S2), we observed an expansion of *Eve* expression domain, while in embryos injected with a higher miR-31 KD concentration (30  $\mu$ M), we observed no change in *Eve* expression (Fig. 2B). This indicates that the higher concentration of miR-31 inhibitor at 30  $\mu$ M, which was used throughout this paper, may trigger *Eve*'s autorepression (Fig. 2B). The exact mechanism of how *Eve* regulates *Vegf3* remains unclear. We speculate that *Vegf3* is likely activated before *Eve* is able to repress its own transcription, since *Vegf3* expression domain expanded in miR-31 KD, *Eve* miR-31 TP, and *Eve* OE, independent of the expression domain of *Eve*. In general, blocking miR-31's suppression of *Eve* resulted in expanded expression domains of most genes tested within our proposed model that impact skeletogenesis (Figs. 1A and 7A). As these genes impact PMC patterning and biomineralization, our results reveal a novel role of *Eve* in sea urchin skeletogenesis.

Previously, it was reported that *Wnt1* is likely to be the ligand for the Fzd5/8-JNK/ROCK signaling pathway (Range et al., 2013). Perturbation of Fzd5/8 or ROCK signaling leads to skeletal defects (Croce et al., 2006). Embryos injected with *Wnt1* miR-31 TP exhibited phenotypes that are relatively less severe than that of miR-31 KD or *Eve* miR-31 TP embryos (Fig. 5A–C). Blocking miR-31's suppression of *Wnt1* resulted in shortened DVCs and body rods that failed to meet posteriorly. However, PMC patterning was mildly affected (Fig. 5B). This may be due to miR-31's weak binding affinity to *Wnt1* compared to *Eve* (Fig. 3). Blocking miR-31's direct suppression of *Wnt1* resulted in an anterior shift in gene expressions in the Veg1 cells (Fig. 7B). Interestingly, *Wnt1* KD causes a vegetal (posterior) shift of expression in *Emx*, (animal ectoderm), *Lim1* (Veg1 ectoderm), *Eve* (Veg1 endoderm and endoderm), *Hox11/13b* (Veg1 endoderm), and *FoxA* (Veg2 mesoderm) (Cui et al., 2014). This indicates that a change in *Wnt1* levels has an impact on Veg1 ectoderm, Veg1 endoderm, and Veg2 mesoderm gene expression domains. While *Wnt1* miR-31 TP embryos exhibit mild phenotypes, embryos overexpressing *Wnt1* CDS resulted in much more severe phenotypes than *Wnt1* miR-31 TP or miR-31 KD embryos, including having supernumerary skeletal rudiments and exogastrulation (Fig. 5D). These incongruous results may be due to *Wnt1*'s possible autoactivation, where overexpression of *Wnt1* would result in even more production of *Wnt1*, resulting in a more severe phenotype. Additionally, overexpression of *Wnt1* would ectopically activate Wnt signaling in all cells, whereas *Wnt1* miR-31 TP only activates Wnt signaling in cells that normally express *Wnt1*. Previous literature indicates that *Wnt1* KD has no effect on PMC patterning, but does result in larvae with a partial gut that lack mouth

formation (Wei et al., 2012). Consistent with previous literature, we observed approximately 50% of all *Wnt1* CDS injected abnormal embryos underwent exogastrulation (Fig. 5D). Overall, results indicate that the anterior shift of *Vegf3* expression due to miR-31's direct suppression of *Wnt1* is not sufficient to fully cause the skeletal and PMC patterning defects observed in miR-31 KD. Nonetheless, proper levels of *Wnt1* are critical for proper skeletal rudiment formation and gastrulation.

Removing the combinatorial suppression of miR-31 on *Eve* and *Wnt1* resulted in skeletal defects and PMC mispatterning (Fig. 6), reminiscent of miR-31 KD induced phenotypes (Stepicheva and Song, 2015) (Fig. 1B). Further, the combination of *Eve* and *Wnt1* miR-31 TPs recapitulated expression domain changes of *Eve*, *Wnt1*, and *Vegf3* in miR-31 KD embryos (Figs. 2B and 7C). This indicates that the expansion in expression of *Vegf3* regulated by *Eve*, along with the anterior shift in *Vegf3* expression domain regulated by *Wnt1*, are potentially the cause of skeletogenic and PMC patterning defects in miR-31 KD embryos.

Consistent with shortened spicules in miR-31 KD embryos, blocking miR-31's suppression of *Eve* and/or *Wnt1* resulted in the downregulation of several PMC-specific biomineralization transcripts (Fig. 8). *P19*, *p58a*, *SM29*, *SM37*, *SM49*, and *SM50* biomineralization transcripts are expressed by the PMCs, present in the biomineral, and may be important for the skeletal mineralization process (Knapp et al., 2012; Mann et al., 2008; Sun and Etensohn, 2014). *P19* is highly expressed in the PMCs during all stages of embryogenesis (Veis, 2011). During the larval stage, *P19*, *p58a*, and *SM50* are expressed in the PMCs that give rise to the larval body rods (Adomako-Ankomah and Etensohn, 2011; Cheers and Etensohn, 2005; Peled-Kamar et al., 2002; Sun and Etensohn, 2014). Results indicate that only *Wnt1* miR-31 TP injected embryos resulted in more than a 3-fold decrease of *p58a*, while both miR-31 KD and *Wnt1* miR-31 TP injected embryos have about a 3-fold decrease of *SM50* compared to the control. Since *p58a* is likely to be involved in depositing the calcite-based biomineral for skeletal synthesis (Adomako-Ankomah and Etensohn, 2011), and accumulation of *SM50* (*LSM34*) is required for initiation of spicule formation and subsequent morphogenesis (Peled-Kamar et al., 2002), their decreased expression may contribute to skeletal shortening and the failure of the tips of the body rods to converge in the miR-31 KD and *Wnt1* miR-31 TP injected embryos. In *Eve* miR-31 TP treated embryos, the only transcript decreased more than 2-fold is *SM37*, which has the same *cis*-regulatory elements as *SM50* and is regulated coordinately with *SM50* throughout development (Lee et al., 1999). However, the function of *SM37* is not known. Similar to *SM37* transcript, *P19*, *SM29*, *SM49*, *MSP130* and *Otop2L* transcripts are expressed in the PMCs, but their exact function in biomineralization is unknown (Leaf et al., 1987; Lee et al., 1999; Livingston et al., 2006; Sun and Etensohn, 2014; Veis, 2011). In miR-31 KD embryos, the composite  $\geq 2$ -fold decrease of *P19*, *SM29*, *SM49*, *SM50* and *Msp130* may all contribute to skeletal defects we observed, since they are expressed in the PMC ventrolateral clusters and in the PMCs at the tips of the larval rods (Sun and Etensohn, 2014). *Wnt1* miR-31 TP resulted in greater than 2-fold decrease in all genes examined, except for *Otop2L*, suggesting that this perturbation has a broad repressive effect on biomineralization and PMC transcripts. Interestingly, it appears that miR-31 may regulate *Eve* and *Wnt1* differently, since the *Wnt1* miR-31 TP has the strongest repressive effects, while the combination of both *Wnt1* and *Eve* miR-31 TPs appears to rescue the *Wnt1* miR-31 TP repressive effect for some biomineralization transcripts (*p58a*, *SM29*, *SM50*, and *Msp130*). These results suggest a complex and undefined regulatory relationship between *Eve* and *Wnt1*. Overall, the decreased trend of these biomineralization and PMC transcripts may partially explain the skeletal defects of shortened DVCs and the larval body rods failing to meet at the posterior end in all the perturbations examined. In addition, the body rods extend from the tri-radiate spicule, and the convergences of the body rods is dependent on its initial orientation (Brandhorst and Davenport, 2001; Gustafson and Wolpert, 1961; McClay et al., 1992). The shortened spicules we observed in miR-31 KD, *Eve* miR-31 TP, *Wnt1* miR-31 TP, and *Eve* + *Wnt1* miR-31 TP could also contribute to the failure of body rod convergence.

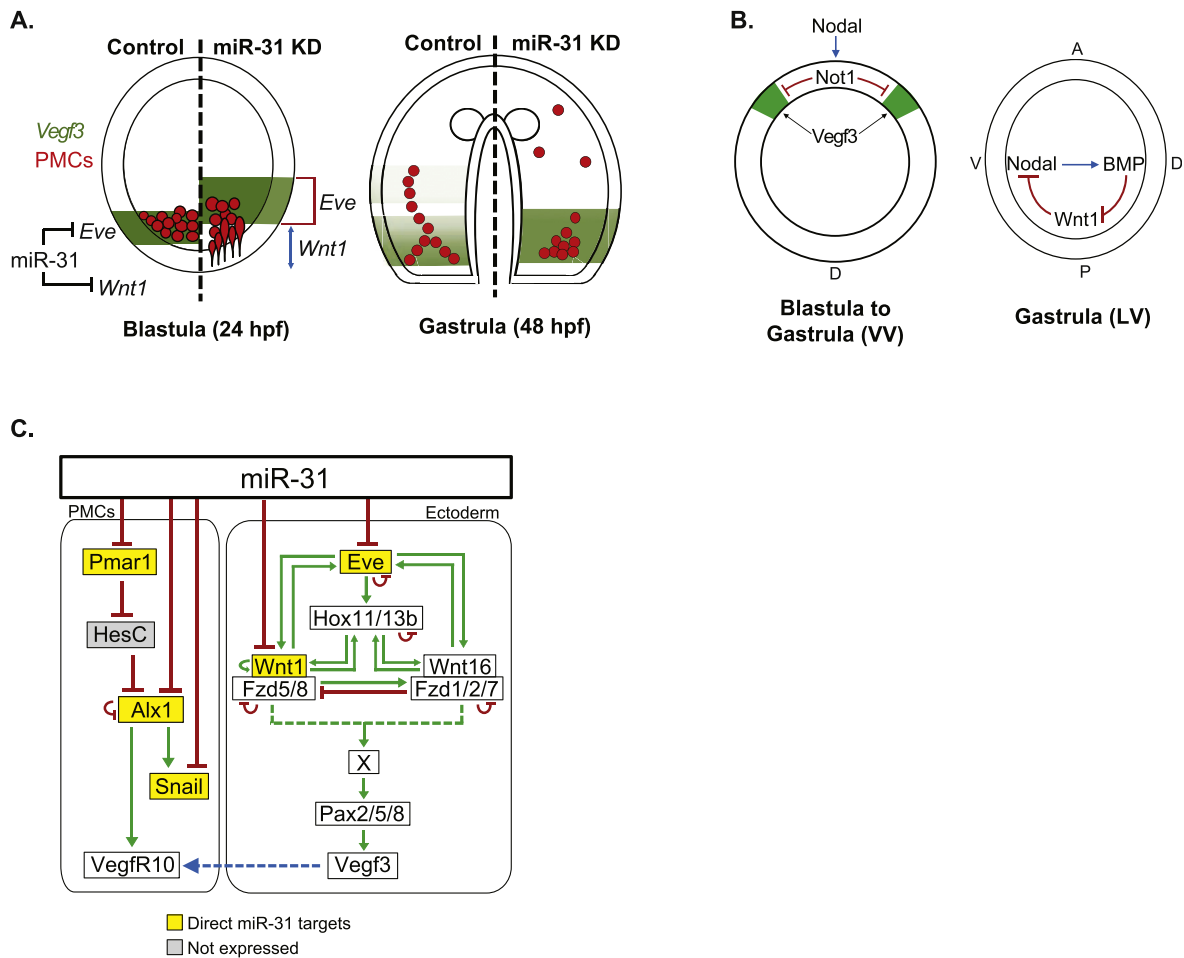


**Fig. 10. miR-31 directly represses components within the PMC GRN and transcripts upstream of Vegf3.** (A) miR-31's regulation of *Eve* and *Wnt1* indirectly impacts *Vegf3* expression in the blastula stage. Removing miR-31's directional suppression of *Eve* results in an expansion of *Vegf3* expression domain, while removing miR-31's direct suppression of *Wnt1* results in an anterior shift of *Vegf3* expression. (B) The expansion of *Vegf3* in the BE-DVM in miR-31 KD embryos could be due to increased *Wnt1*, thus increasing *Wnt1*'s restriction of *Nodal* from the posterior-ventral region during gastrula stage. Decreased *Nodal* would result in less *Not1* expression, leading to less *Vegf3* restriction in the BE-DVM. VV = Ventral view; LV = Lateral view; A = anterior; P = posterior; V = ventral; D = dorsal. (C) We previously identified miR-31 to directly suppress *Pmar1*, *Alx1* and *Snail*, which are expressed in the PMCs (Stepicheva and Song, 2015). cWnt/ $\beta$ -catenin triggers specification of PMCs by activating the transcriptional repressor *Pmar1* expressed exclusively in the micromeres. *Pmar1* inhibits transcriptional repressor *HesC* (Guss and Etensohn, 1997; Oliveri et al., 2003; Revilla-i-Domingo et al., 2007). This leads to the activation of *Alx1*, which in turn, activates *Snail* and *VegfR10* (Etensohn et al., 2003; Rafiq et al., 2012; Sharma and Etensohn, 2011). *VegfR10* is expressed by the PMCs and is thought to respond to the *Vegf3* ligand secreted by the ectoderm to guide patterning of PMCs. In this study, we identified *Eve* and *Wnt1* as direct miR-31 targets upstream of *Vegf3* activation.

Removal of miR-31's suppression of *Eve* and *Wnt1* resulted in an expansion and anterior shift in *Vegf3*'s expression domain which correlated with PMC migration defects. *Vegf3* plays an especially critical role in PMC patterning. Previous research indicates that *Vegf3* KD embryos have increased *Vegf3* expression and mispatterned PMCs in the posterior end of the embryo with a loss of skeleton (Adomako-Ankomah and Etensohn, 2013; Duloquin et al., 2007). This PMC patterning defect is similar in miR-31 KD embryos, where expanded *Vegf3* expression potentially contributes to the PMC positioning defect (Stepicheva and Song, 2015). In the current study, we observed that *VegfR10*-expressing PMCs in miR-31 KD blastulae had delayed PMC ingress (Fig. 9A). Normally, PMCs are fully ingressed into the blastocoel by the mesenchyme blastula stage (24 hpf) (Bradham et al., 2004; Sun and Etensohn, 2014; Wu et al., 2007). In miR-31 KD embryos, only 67% of the *VegfR10*-expressing PMCs have fully ingressed by 26 hpf. This consistent delay in ingress may contribute to the PMC positioning defects and shortened skeletal spicules, but exactly how miR-31 regulates ingress is not known. Additionally, *Vegf3* is expressed in a gradient in the normal sea urchin gastrulae (Adomako-Ankomah and Etensohn, 2013; Duloquin

et al., 2007), similar to *VEGF-A* in vertebrates (Chauvet et al., 2013). We observed PMC anterior migration correlates with *Vegf3* expression (Fig. 9B). Interestingly, in miR-31 KD blastulae (24 hpf), *Vegf3* expression domain was expanded in the AP axis compared to control TP; however, by 40 hpf, *Vegf3* expanded expression shifted from the AP to the DV axis (Fig. 9B and C). Since the expression of BE genes, such as *Vegf3*, is restricted by expression of *Nodal* and *BMP* in the DVM (McIntyre et al., 2013), the expansion of *Vegf3* expression in the DV axis may be explained by the regulatory relationship between *Wnt1*, *Nodal*, and *BMP* signaling. During early cleavage stages (60-cell), *Wnt1* indirectly activates *Nodal* by suppressing *FoxQ2* to specify the AP axis (Range et al., 2013; Yaguchi et al., 2008). In the gastrula stage, *Nodal* activates *BMP* signaling to restrict *Wnt1* to the posterior-ventral side (Duboc et al., 2010; Lapraz et al., 2009; Wei et al., 2012) (Fig. 10B). Later in the gastrula stage, *Wnt1* prevents *Nodal* expression in the posterior region to establish the ciliary band in the DV axis (Wei et al., 2012). In turn, *Nodal* activates *Not1*, which represses *Vegf3* in the ventral ectoderm and restricts *Vegf3*'s expression to the two lateral ectodermal domains and posterior ventral corners (BE-DVM) (Layout, 2020; Li et al., 2012; McIntyre et al., 2013).

In miR-31 KD blastulae, we observed *Wnt1* is expanded in the AP axis and shifted anteriorly compared to injected control embryos (Figs. 2 and 9B). During gastrulation, this miR-31 KD-induced ectopic expression of *Wnt1* may restrict *Nodal* and *Not1* in the ventral ectoderm, resulting in expanded *Vegf3* expression in the DV axis (Figs. 9C and 10B). The fine-tuning nature of miRNAs would not likely result in a dramatic loss of BE-DVM restriction, but rather a slight expansion of *Vegf3*. Currently, we do not know the exact mechanism of how miR-31 mediates the shift in *Vegf3* expression expansion from AP to DV axis; we speculate that this may involve cross-regulation of *Wnt1*, *Nodal* and BMP signaling.

Overall, this study identifies miR-31's direct suppression of *Eve* and *Wnt1* to be a potential underlying molecular mechanism of miR-31's regulation of *Vegf3* expression and skeletogenesis (Fig. 10A). miR-31's suppression of *Eve* and *Wnt1* defines the expression domain of *Vegf3*, which in turn, regulates skeletogenesis and PMC patterning. miR-31's direct repression of *Wnt1* may indirectly affect the expansion of *Vegf3* in the DV axis, potentially via *Wnt1*'s regulation of *Nodal* which activates *Not1* to restrict *Vegf3* expression in the ventral ectoderm (Fig. 10B). Previously, we identified miR-31 to directly repress major TFs within the PMC GRN, such as *Pmar1*, *Alx1*, and *Snail*, in addition to a not well understood *Vegf* receptor, *VegfR7* (Fig. 10C). Upon  $\beta$ -catenin activation in the micromeres, *Pmar1* is activated in the PMC GRN. It represses a ubiquitously expressed repressor *HesC* (Guss and Etensohn, 1997; Oliveri et al., 2003; Revilla-i-Domingo et al., 2007). Hence, *HesC* in the micromeres is repressed, allowing transcriptional activation of *Alx1*. *Alx1* plays a central role in the PMC GRN by activating multiple TFs such as *Snail*, which is important for PMC EMT, and *VegfR10* (Etensohn et al., 2003; Khor et al., 2019; Rafiq et al., 2012; Sharma and Etensohn, 2011). Removal of miR-31's direct suppression of *Alx1* and/or *VegfR7* resulted in shorter skeletal spicules and mispatterned PMCs (Stepicheva and Song, 2015). Thus, our previous and current finding indicate that miR-31 suppresses the PMC GRN components, *Eve*, and *Wnt1* to ensure proper skeletogenesis and PMC patterning.

## Acknowledgements

The authors would like to thank David McClay (Duke University) for his kind gift of 1D5 antibody. We also thank Dr. Ryan Range (Auburn University) for the *Wnt16* plasmid. This work is funded by University of Delaware Graduate Fellowship to NFS. NSF CAREER (IOS 1553338) to JLS and NIH NIGMS P20GM103446. We thank members of the Song lab in careful reading of the manuscript. The authors thank the anonymous reviewers for their invaluable comments.

## Appendix A. Supplementary data

Supplementary data to this article can be found online at <https://doi.org/10.1016/j.ydbio.2021.01.008>.

## References

Adomako-Ankomah, A., Etensohn, C.A., 2011. P58-A and P58-B: novel proteins that mediate skeletogenesis in the sea urchin embryo. *Dev. Biol.* 353, 81–93.

Adomako-Ankomah, A., Etensohn, C.A., 2013. Growth factor-mediated mesodermal cell guidance and skeletogenesis during sea urchin gastrulation. *Development* 140, 4214–4225.

Adomako-Ankomah, A., Etensohn, C.A., 2014. Growth factors and early mesoderm morphogenesis: insights from the sea urchin embryo. *Genesis* 52, 158–172.

Anstrom, J.A., 1992. Microfilaments, cell shape changes, and the formation of primary mesenchyme in sea urchin embryos. *J. Exp. Zool.* 264, 312–322.

Bartel, D.P., 2009. MicroRNAs: target recognition and regulatory functions. *Cell* 136, 215–233.

Bartel, D.P., 2018. Metazoan MicroRNAs. *Cell* 173, 20–51.

Bradham, C.A., Miranda, E.L., McClay, D.R., 2004. PI3K inhibitors block skeletogenesis but not patterning in sea urchin embryos. *Dev. Dynam.* 229, 713–721.

Brandhorst, B.P., Davenport, R., 2001. Skeletogenesis in sea urchin interordinal hybrid embryos. *Cell Tissue Res.* 305, 159–167.

Chauvet, S., Burk, K., Mann, F., 2013. Navigation rules for vessels and neurons: cooperative signaling between VEGF and neural guidance cues. *Cell. Mol. Life Sci.* 70, 1685–1703.

Cheers, M.S., Etensohn, C.A., 2004. Rapid microinjection of fertilized eggs. *Methods Cell Biol.* 74, 287–310.

Cheers, M.S., Etensohn, C.A., 2005. P16 is an essential regulator of skeletogenesis in the sea urchin embryo. *Dev. Biol.* 283, 384–396.

Croce, J., Duloquin, L., Lhomond, G., McClay, D.R., Gache, C., 2006. Frizzled5/8 is required in secondary mesenchyme cells to initiate archenteron invagination during sea urchin development. *Development* 133, 547–557.

Cui, M., Siriwon, N., Li, E., Davidson, E.H., Peter, I.S., 2014. Specific functions of the Wnt signaling system in gene regulatory networks throughout the early sea urchin embryo. *Proc. Natl. Acad. Sci. U. S. A.* 111, E5029–E5038.

Cui, M., Vielmas, E., Davidson, E.H., Peter, I.S., 2017. Sequential response to multiple developmental network circuits encoded in an intronic cis-regulatory module of sea urchin *hox11/13b*. *Cell Rep.* 19, 364–374.

Duboc, V., Lapraz, F., Saudemont, A., Bessodes, N., Mekpoh, F., Haillet, E., Quirin, M., Lepage, T., 2010. *Nodal* and *BMP2/4* pattern the mesoderm and endoderm during development of the sea urchin embryo. *Development* 137, 223–235.

Duboc, V., Rottinger, E., Besnardeau, L., Lepage, T., 2004. *Nodal* and *BMP2/4* signaling organizes the oral-aboral axis of the sea urchin embryo. *Dev. Cell* 6, 397–410.

Duloquin, L., Lhomond, G., Gache, C., 2007. Localized VEGF signaling from ectoderm to mesenchyme cells controls morphogenesis of the sea urchin embryo skeleton. *Development* 134, 2293–2302.

Etensohn, C.A., 1999. Cell movements in the sea urchin embryo. *Curr. Opin. Genet. Dev.* 9, 461–465.

Etensohn, C.A., Adomako-Ankomah, A., 2019. The evolution of a new cell type was associated with competition for a signaling ligand. *PLoS Biol.* 17, e3000460.

Etensohn, C.A., Illies, M.R., Oliveri, P., De Jong, D.L., 2003. *Alx1*, a member of the *Cart1/Alx3/Alx4* subfamily of Paired-class homeodomain proteins, is an essential component of the gene network controlling skeletogenic fate specification in the sea urchin embryo. *Development* 130, 2917–2928.

Etensohn, C.A., McClay, D.R., 1986. The regulation of primary mesenchyme cell migration in the sea urchin embryo: transplantations of cells and latex beads. *Dev. Biol.* 117, 380–391.

Fink, R.D., McClay, D.R., 1985. Three cell recognition changes accompany the ingression of sea urchin primary mesenchyme cells. *Dev. Biol.* 107, 66–74.

Gregory, P.A., Bert, A.G., Paterson, E.L., Barry, S.C., Tsykin, A., Farshid, G., Vadas, M.A., Khew-Goodall, Y., Goodall, G.J., 2008. The miR-200 family and miR-205 regulate epithelial to mesenchymal transition by targeting ZEB1 and SIP1. *Nat. Cell Biol.* 10, 593–601.

Guss, K.A., Etensohn, C.A., 1997. Skeletal morphogenesis in the sea urchin embryo: regulation of primary mesenchyme gene expression and skeletal rod growth by ectoderm-derived cues. *Development* 124, 1899–1908.

Gustafson, T., Wolpert, L., 1961. Studies on the cellular basis of morphogenesis in the sea urchin embryo. Directed movements of primary mesenchyme cells in normal and vegetalized larvae. *Exp. Cell Res.* 24, 64–79.

Hughes, I., Blasiole, B., Huss, D., Warchol, M.E., Rath, N.P., Hurl, B., Ignatova, E., Dickman, J.D., Thalmann, R., Levenson, R., Ornitz, D.M., 2004. Otopetrin 1 is required for otolith formation in the zebrafish *Danio rerio*. *Dev. Biol.* 276, 391–402.

Hurl, B., Ignatova, E., Massironi, S.M., Mashimo, T., Rios, X., Thalmann, I., Thalmann, R., Ornitz, D.M., 2003. Non-syndromic vestibular disorder with otoconial agenesis in tilted/mergulador mice caused by mutations in otopetrin 1. *Hum. Mol. Genet.* 12, 777–789.

Jan, C.H., Friedman, R.C., Ruby, J.G., Bartel, D.P., 2011. Formation, regulation and evolution of *Caenorhabditis elegans* 3'UTRs. *Nature* 469, 97–101.

Katow, H., 2015. Mechanisms of the epithelial-to-mesenchymal transition in sea urchin embryos. *Tissue Barriers* 3, e1059004.

Katow, H., Solorsh, M., 1981. Ultrastructural and time-lapse studies of primary mesenchyme cell behavior in normal and sulfate-deprived sea urchin embryos. *Exp. Cell Res.* 136, 233–245.

Khor, J.M., Guerrero-Santoro, J., Etensohn, C.A., 2019. Genome-wide Identification of Binding Sites and Gene Targets of *Alx1*, a Pivotal Regulator of Echinoderm Skeletogenesis. *Development*.

Khorshid, M., Hausser, J., Zavolan, M., van Nimwegen, E., 2013. A biophysical miRNA-mRNA interaction model infers canonical and noncanonical targets. *Nat. Methods* 10, 253–255.

Kim, J., Siverly, A.N., Chen, D., Wang, M., Yuan, Y., Wang, Y., Lee, H., Zhang, J., Muller, W.J., Liang, H., Gan, B., Yang, X., Sun, Y., You, M.J., Ma, L., 2016. Ablation of miR-10b suppresses oncogene-induced mammary tumorigenesis and metastasis and reactivates tumor-suppressive pathways. *Canc. Res.* 76, 6424–6435.

Knapp, R.T., Wu, C.H., Mobilia, K.C., Joester, D., 2012. Recombinant sea urchin vascular endothelial growth factor directs single-crystal growth and branching in vitro. *J. Am. Chem. Soc.* 134, 17908–17911.

Lapraz, F., Besnardeau, L., Lepage, T., 2009. Patterning of the dorsal-ventral axis in echinoderms: insights into the evolution of the BMP-chordin signaling network. *PLoS Biol.* 7, e1000248.

Layous, M., 2020. In: Khalaily, L. (Ed.), *The Tolerance to Hypoxia Is Defined by a Time-Sensitive Response of the Gene Regulatory Network in Sea Urchin Embryos*.

Leaf, D.S., Anstrom, J.A., Chin, J.E., Harkey, M.A., Showman, R.M., Raff, R.A., 1987. Antibodies to a fusion protein identify a cDNA clone encoding msp130, a primary mesenchyme-specific cell surface protein of the sea urchin embryo. *Dev. Biol.* 121, 29–40.

Lee, Y.H., Britten, R.J., Davidson, E.H., 1999. SM37, a skeletogenic gene of the sea urchin embryo linked to the SM50 gene. *Dev. Growth Differ.* 41, 303–312.

Li, E., Materna, S.C., Davidson, E.H., 2012. Direct and indirect control of oral ectoderm regulatory gene expression by *Nodal* signaling in the sea urchin embryo. *Dev. Biol.* 369, 377–385.

- Livingston, B.T., Killian, C.E., Wilt, F., Cameron, A., Landrum, M.J., Ermolaeva, O., Sapojnikov, V., Maglott, D.R., Buchanan, A.M., Etensohn, C.A., 2006. A genome-wide analysis of biomineralization-related proteins in the sea urchin *Strongylocentrotus purpuratus*. *Dev. Biol.* 300, 335–348.
- Lyons, D.C., Kaltenbach, S.L., McClay, D.R., 2012. Morphogenesis in sea urchin embryos: linking cellular events to gene regulatory network states, 1. *Wiley Interdiscip Rev Dev Biol*, pp. 231–252.
- Mann, K., Poustka, A.J., Mann, M., 2008. The sea urchin (*Strongylocentrotus purpuratus*) test and spine proteomes. *Proteome Sci.* 6, 22.
- Martínez-Bartolomé, M., Range, R.C., 2019. A Biphasic Role of Non-canonical Wnt16 Signaling during Early Anterior-Posterior Patterning and Morphogenesis of the Sea Urchin Embryo, vol. 146. *Development*.
- McClay, D.R., Armstrong, N.A., Hardin, J., 1992. Pattern formation during gastrulation in the sea urchin embryo. *Dev. Suppl.* 33–41.
- McClay, D.R., Cannon, G.W., Wessel, G.M., Fink, R.D., Marchase, R.B., 1983. Patterns of antigenic expression in early sea urchin development. In: Raff, W.R.J.a.R.A. (Ed.), *Time, Space, and Pattern in Embryonic Development*. A.R. Liss, New York, pp. 157–169.
- McIntyre, D.C., Lyons, D.C., Martik, M., McClay, D.R., 2014. Branching out: origins of the sea urchin larval skeleton in development and evolution. *Genesis* 52, 173–185.
- McIntyre, D.C., Seay, N.W., Croce, J.C., McClay, D.R., 2013. Short-range Wnt5 signaling initiates specification of sea urchin posterior ectoderm. *Development* 140, 4881–4889.
- Mikels, A.J., Nusse, R., 2006. Purified Wnt5a protein activates or inhibits beta-catenin-TCF signaling depending on receptor context. *PLoS Biol.* 4, e115.
- Morgulis, M., Gildor, T., Roopin, M., Sher, N., Malik, A., Lalzar, M., Dines, M., Ben-Tabou de-Leon, S., Khalaily, L., 2019. Possible cooption of a VEGF-driven tubulogenesis program for biomineralization in echinoderms. *Proc. Natl. Acad. Sci. U. S. A.* 116, 12353–12362.
- Nakajima, Y., Burke, R.D., 1996. The initial phase of gastrulation in sea urchins is accompanied by the formation of bottle cells. *Dev. Biol.* 179, 436–446.
- Nishita, M., Enomoto, M., Yamagata, K., Minami, Y., 2010a. Cell/tissue-tropic functions of Wnt5a signaling in normal and cancer cells. *Trends Cell Biol.* 20, 346–354.
- Nishita, M., Itsukushima, S., Nomachi, A., Endo, M., Wang, Z., Inaba, D., Qiao, S., Takada, S., Kikuchi, A., Minami, Y., 2010b. Ror2/Frizzled complex mediates Wnt5a-induced AP-1 activation by regulating Dishevelled polymerization. *Mol. Cell Biol.* 30, 3610–3619.
- Oliveri, P., Davidson, E.H., McClay, D.R., 2003. Activation of pmar1 controls specification of micromeres in the sea urchin embryo. *Dev. Biol.* 258, 32–43.
- Pedrioli, D.M., Karpanen, T., Dabouras, V., Jurisic, G., van de Hoek, G., Shin, J.W., Marino, D., Kälin, R.E., Leidel, S., Cinelli, P., Schulte-Merker, S., Brändli, A.W., Detmar, M., 2010. miR-31 functions as a negative regulator of lymphatic vascular lineage-specific differentiation in vitro and vascular development in vivo. *Mol. Cell Biol.* 30, 3620–3634.
- Peled-Kamar, M., Hamilton, P., Wilt, F.H., 2002. Spicule matrix protein LSM34 is essential for biomineralization of the sea urchin spicule. *Exp. Cell Res.* 272, 56–61.
- Peter, I.S., Davidson, E.H., 2010. The endoderm gene regulatory network in sea urchin embryos up to mid-blastula stage. *Dev. Biol.* 340, 188–199.
- Peter, I.S., Davidson, E.H., 2011. A gene regulatory network controlling the embryonic specification of endoderm. *Nature* 474, 635–639.
- Rafiq, K., Cheers, M.S., Etensohn, C.A., 2012. The genomic regulatory control of skeletal morphogenesis in the sea urchin. *Development* 139, 579–590.
- Rafiq, K., Shashikant, T., McManus, C.J., Etensohn, C.A., 2014. Genome-wide analysis of the skeletogenic gene regulatory network of sea urchins. *Development* 141, 950–961.
- Range, R.C., 2018. Canonical and non-canonical Wnt signaling pathways define the expression domains of Frizzled 5/8 and Frizzled 1/2/7 along the early anterior-posterior axis in sea urchin embryos. *Dev. Biol.* 444, 83–92.
- Range, R.C., Angerer, R.C., Angerer, L.M., 2013. Integration of canonical and noncanonical Wnt signaling pathways patterns the neuroectoderm along the anterior-posterior axis of sea urchin embryos. *PLoS Biol.* 11, e1001467.
- Ransick, A., Rast, J.P., Minokawa, T., Calestani, C., Davidson, E.H., 2002. New early zygotic regulators expressed in endomesoderm of sea urchin embryos discovered by differential array hybridization. *Dev. Biol.* 246, 132–147.
- Remsburg, C., Konrad, K., Sampilo, N.F., Song, J.L., 2019. Analysis of microRNA functions. *Methods Cell Biol.* 151, 323–334.
- Revilla-i-Domingo, R., Oliveri, P., Davidson, E.H., 2007. A missing link in the sea urchin embryo gene regulatory network: hesC and the double-negative specification of micromeres. *Proc. Natl. Acad. Sci. U. S. A.* 104, 12383–12388.
- Rizzo, F., Fernandez-Serra, M., Squarzone, P., Archimandritis, A., Arnone, M.I., 2006. Identification and developmental expression of the ets gene family in the sea urchin (*Strongylocentrotus purpuratus*). *Dev. Biol.* 300, 35–48.
- Rottinger, E., Saudemont, A., Duboc, V., Besnardeau, L., McClay, D., Lepage, T., 2008. FGF signals guide migration of mesenchymal cells, control skeletal morphogenesis [corrected] and regulate gastrulation during sea urchin development. *Development* 135, 353–365.
- Rozen, S., Skaletsky, H., 2000. Primer3 on the WWW for general users and for biologist programmers. *Methods Mol. Biol.* 132, 365–386.
- Sampilo, N.F., Stepicheva, N.A., Zaidi, S.A.M., Wang, L., Wu, W., Wikramanayake, A., Song, J.L., 2018. Inhibition of microRNA Suppression of, vol. 145. *Development*.
- Schlessinger, J., 2000. Cell signaling by receptor tyrosine kinases. *Cell* 103, 211–225.
- Sharma, T., Etensohn, C.A., 2011. Regulative deployment of the skeletogenic gene regulatory network during sea urchin development. *Development* 138, 2581–2590.
- Staton, A.A., Giraldez, A.J., 2011. Use of target protector morpholinos to analyze the physiological roles of specific miRNA-mRNA pairs in vivo. *Nat. Protoc.* 6, 2035–2049.
- Stepicheva, N., Nigam, P.A., Siddam, A.D., Peng, C.F., Song, J.L., 2015. microRNAs regulate beta-catenin of the Wnt signaling pathway in early sea urchin development. *Dev. Biol.* 402, 127–141.
- Stepicheva, N.A., Song, J.L., 2014. High throughput microinjections of sea urchin zygotes. *JoVE*, e50841.
- Stepicheva, N.A., Song, J.L., 2015. microRNA-31 modulates skeletal patterning in the sea urchin embryo. *Development* 142, 3769–3780.
- Sun, Z., Etensohn, C.A., 2014. Signal-dependent regulation of the sea urchin skeletogenic gene regulatory network. *Gene Expr. Patterns* 16, 93–103.
- Söllner, C., Schwarz, H., Geisler, R., Nicolson, T., 2004. Mutated otopetrin 1 affects the genesis of otoliths and the localization of Starmaker in zebrafish. *Dev. Gene. Evol.* 214, 582–590.
- Valastyan, S., Weinberg, R.A., 2010. miR-31: a crucial overseer of tumor metastasis and other emerging roles. *Cell Cycle* 9, 2124–2129.
- Weis, A., 2011. Organic matrix-related mineralization of sea urchin spicules, spines, test and teeth. *Front. Biosci.* 16, 2540–2560.
- Wei, Z., Range, R., Angerer, R., Angerer, L., 2012. Axial patterning interactions in the sea urchin embryo: suppression of nodal by Wnt1 signaling. *Development* 139, 1662–1669.
- Wu, S.Y., Ferkowicz, M., McClay, D.R., 2007. Ingression of primary mesenchyme cells of the sea urchin embryo: a precisely timed epithelial mesenchymal transition. *Birth Defects Res C Embryo Today* 81, 241–252.
- Yaguchi, S., Yaguchi, J., Angerer, R.C., Angerer, L.M., 2008. A Wnt-FoxQ2-nodal pathway links primary and secondary axis specification in sea urchin embryos. *Dev. Cell* 14, 97–107.
- Yu, T., Ma, P., Wu, D., Shu, Y., Gao, W., 2018. Functions and mechanisms of microRNA-31 in human cancers. *Biomed. Pharmacother.* 108, 1162–1169.